Reflection seismic profiles of the core-mantle boundary

A. R. Ross and H. Thybo
Geological Institute, University of Copenhagen, Copenhagen, Denmark

L. N. Solidilov
Center for Regional Geophysical and Geoecological Studies, Moscow, Russia

Received 21 March 2003; revised 15 April 2004; accepted 11 June 2004; published 11 August 2004.

[1] High amplitude, high frequency, and laterally coherent seismic phases from the core-mantle boundary (CMB) are observed on data from Peaceful Nuclear Explosions in Siberia. These arrivals are observed at 2600–4000 km offset with travel times and move-outs consistent with CMB reflections (*PcP*) and are readily correlated because of the small station interval of 10 km. The duration and complexity of the arrivals are inconsistent with a simple reflection from a single CMB interface. They require the combination of *PcP* and a complex precursor phase (*PdP*) from the top of an ultralow-velocity zone (ULVZ) despite the fact that earthquake recordings indicate that there is no ULVZ present beneath this part of Siberia. Lateral variations in the waveform imply that the thickness and physical properties of the ULVZ change with a wavelength of 150–200 km and an amplitude of up to 8 km. We find at least one location where there is no ULVZ present. At another well-sampled location, the precursor has higher frequency content than the primary arrival. Reflectivity modeling of these *PcP*/*PdP* phases shows that kilometer-scale layering may be required in the ULVZ to explain the seismic waveform and the frequency split. The modeling shows very low velocity in the ULVZ with reductions of 25 and 40% for *P* and *S* waves, respectively. This indicates higher percentages of partial melt in the ULVZ than hitherto interpreted. Our observations indicate that the ULVZ may be present over wide areas of the Earth with a thickness below the resolution limit of seismological data with a lower frequency content. *INDEX TERMS:* 7207 Seismology: Core and mantle; 7219 Seismology: Nuclear explosion seismology; 7203 Seismology: Body wave propagation; *KEYWORDS:* core-mantle boundary, ultralow velocity zone, nuclear explosion

Citation: Ross, A. R., H. Thybo, and L. N. Solidilov (2004), Reflection seismic profiles of the core-mantle boundary, *J. Geophys. Res.*, *109*, B08303, doi:10.1029/2003JB002515.

1. Introduction

[2] The core-mantle boundary (CMB) is the major physical discontinuity within the Earth and the lower boundary layer of the mantle and may be an important region for the driving forces of plate tectonics as the possible source of mantle plumes. Accordingly, the details of the transition between the core and mantle have in recent years received considerable attention. In part, this has been motivated by tomographic images which suggest that velocity anomalies may extend throughout the mantle between the core-mantle boundary and the base of the lithosphere [*Grand et al.*, 1997; *van der Hilst et al.*, 1997] and by a significant amount of research on the chemical properties of the lower mantle with, e.g., diamond anvil cells [*Knittle*, 1998]. The importance of the CMB region to the whole dynamics of the mantle is reflected in the suggestion that plumes may originate from the boundary layer between the core and mantle [*Helmberger et al.*, 1998]. However, even the highest-resolution tomographic images lack the resolution to identify short-scale (<200–300 km) velocity anomalies at the base of the mantle. Fortunately, other types of analysis of seismic waves from both earthquakes and, as we report here, controlled source profiles provide the high vertical and horizontal resolution needed to study the fine structure at the CMB.

[3] Detailed seismological investigations of the lowermost mantle have discovered the existence of a 5–50 km thick ultralow velocity zone (ULVZ) at the core-mantle boundary [*Garnero and Helmberger*, 1995; *Mori and Helmberger*, 1995; *Revenaugh and Meyer*, 1997; *Garnero et al.*, 1998]. The velocity reduction reported in this ULVZ is 5–20% for compressional waves and 10–50% for shear waves as compared to the lower mantle above. To date, less than half of the CMB has been investigated for the existence of an ULVZ, and it is observed in only 12% of the locations studied [*Garnero and Jeanloz*, 2000]. The CMB has been investigated with several seismic phases (*SPdKS* [*Garnero et al.*, 1993; *Garnero and Helmberger*, 1995, 1996; *Helmberger et al.*, 1998; *Williams et al.*, 1998; *Helmberger et al.*, 2000], *PKP* [*Vidale and Hedlin*, 1998; *Wen and Helmberger*, 1998], *ScP* [*Garnero and Vidale*, 1999; *Castle and van der Hilst*, 2000; *Reasoner and Revenaugh*, 2000;

0148-0227/04/2003JB002515$09.00

Rost and Revenaugh, 2001], *SKS* [*Stutzmann et al.*, 2000] and *PcP* [*Mori and Helmberger*, 1995; *Revenaugh and Meyer*, 1997; *Williams et al.*, 1998]) as well as travel times [*Sylvander and Souriau*, 1996; *Sylvander et al.*, 1997]. These studies have identified the ULVZ in many locations around the world and suggest that the ULVZ may be a layer of partially molten lower mantle material [*Williams and Garnero*, 1996; *Vidale and Hedlin*, 1998; *Wen and Helmberger*, 1998]. However, the seismic data are also consistent with a transition layer between the core and mantle containing a mixture of core and mantle material [*Garnero and Jeanloz*, 2000] or a layer of volatile "sediments" produced from the small percentage of silicates present in the core after rising to the top of the outer core to form a layer below the traditional definition of the CMB [*Buffett et al.*, 2000]. Where observed, the ULVZ shows considerable variability in thickness over distances of only a few hundred kilometers with thicknesses ranging from 5 to 40 km [*Williams and Garnero*, 1996; *Wysession et al.*, 1999].

[4] The studies mentioned above have relied on natural earthquake sources to sample the CMB region. This has resulted in particularly good coverage of the CMB in certain regions (e.g., the Pacific Ocean [*Garnero et al.*, 1998]) where high seismic station density and high earthquake frequency at the appropriate offsets coincide. There is poorer coverage in other regions which do not have appropriately located stations and sources. One of those poorly sampled regions is the former Soviet Union. Here we present high-resolution, high-frequency seismic data from nuclear sources which suggest the existence of a very thin ULVZ at two locations beneath Siberia in a region where no ULVZ has been previously reported. The offset range is between 20° and 40°, which is at the limit at which *PcP* has a high enough reflection coefficient to be visible [*Kampfmann and Mueller*, 1989; *Astiz et al.*, 1996]. Our findings raise the possibility that an ULVZ may be present over a wide area of the Earth with a thickness below the resolution limit of most seismological techniques.

[5] Siberia is not entirely unexplored in terms of lower mantle and CMB structure. The lowermost mantle under Siberia has been examined in several studies of earthquake *P* wave data from the Pacific subduction zones recorded at various sites in western Europe [*Weber and Davis*, 1990; *Gaherty and Lay*, 1992; *Weber*, 1993; *Thomas and Weber*, 1997; *Thomas et al.*, 1998; *Freybourger et al.*, 1999, 2001; *Thomas et al.*, 2002]. The reflection points for *PcP* are clustered around 80°E mostly under Siberia and the Kara Sea, east of the trace of the Ural Mountains and north of the location of the Peaceful Nuclear Explosion profiles. These studies show *PcP* precursors which arrive 10 s ahead of *PcP* and correspond to reflections from the top of D″. There are no reports of precursors arriving from 5 to 2 s before *PcP*, which is the expected arrival time of reflections from the top of an ULVZ at the offset range of 75°–80° for these earthquakes and the European recording stations used.

2. Peaceful Nuclear Explosions

[6] The Soviet Peaceful Nuclear Explosion (PNE) program operated between 1965 and 1988 and in this time generated a set of long-range seismic profiles which is unique in two respects. First, the sources are physically very small and compact with high energy output and a precise location and onset time. Second, the sources were recorded to very large offsets and long travel times with very closely spaced seismometers. This allows for reliable correlation of seismic phases with a very compact source waveform.

[7] In total, there were 122 nuclear detonations for engineering, construction, and geoscientific purposes as part of the PNE program [*Sultanov et al.*, 1999]. The specifically geophysical part of this program accounted for 41 of these explosions which were typically fired in deep boreholes at depths of around 0.5–1 km, although some shots were detonated in mines. The shots were recorded by arrays of Russian-made Taiga short-period three-component seismographs which were deployed at a 10–15 km spacing along profiles with maximum offsets of 3000–4000 km. The yield of the PNE shots was sufficient (up to earthquake equivalent 5.6 m_b) for recording of seismic energy outside of the former Soviet Union on the global seismograph network and on seismic arrays such as NORSAR and Gräfenberg. Three components of ground displacement were recorded by the Taiga instruments. All the PNE data were originally recorded as analogue data which were digitized in the 1990s from the original tapes. These digitized data have been made available to a limited number of groups outside Russia.

[8] Previous interpretations of the PNE data have concentrated on the original purpose of the experiments, which was to investigate the mantle and mantle transition zones beneath Siberia [*Fuchs*, 1997; *Thybo and Perchuc*, 1997; *Nielsen et al.*, 1999; *Ryberg and Wenzel*, 1999; *Morozova et al.*, 2000; *Nielsen et al.*, 2002; *Thybo et al.*, 2003a]. Typical record lengths were 1100 s; long enough to allow observation of arrivals from the lower mantle and the core in addition to the primary targets of upper mantle discontinuities. The lack of earthquake sources in the very large area covered by Siberia makes the PNE data particularly interesting since they allow observations of the Earth's structure at offsets and locations where it would not be possible with natural sources.

[9] Our analysis is based on seismic recordings of three PNE shots: KRATON-1 and KRATON-4 detonated in 1978 and BATHOLITH-2 detonated in 1980 [*Egorkin*, 1999; *Sultanov et al.*, 1999] (Figure 1). We have not found any indication of arrivals from the CMB in the other PNE record sections that are available to us (METEORITE, QUARTZ, and KIMBERLITE profiles). This is a result of inappropriate offset ranges. For example, we do not see any CMB arrivals on recordings of shots KRATON-2 and KRATON-3 which are in the center of the profile and do not have offsets >20°. In this offset range the signal-to-noise ratio is too low to observe *PcP* [*Astiz et al.*, 1996]. However, *PcP* arrivals from KRATON-3 are observed on the NORSAR network in Norway, suggesting that these shots have sufficient energy to produce CMB reflections if observed at the appropriate offset range.

[10] Profile KRATON is located in Siberia, stretching from the Ural Mountains to the Sea of Okhotsk. Four individual PNEs and a number of much smaller chemical explosions were recorded by the instruments along the profile. Only the two PNEs at the ends of the profile are discussed here, as the other two split-spread shots have

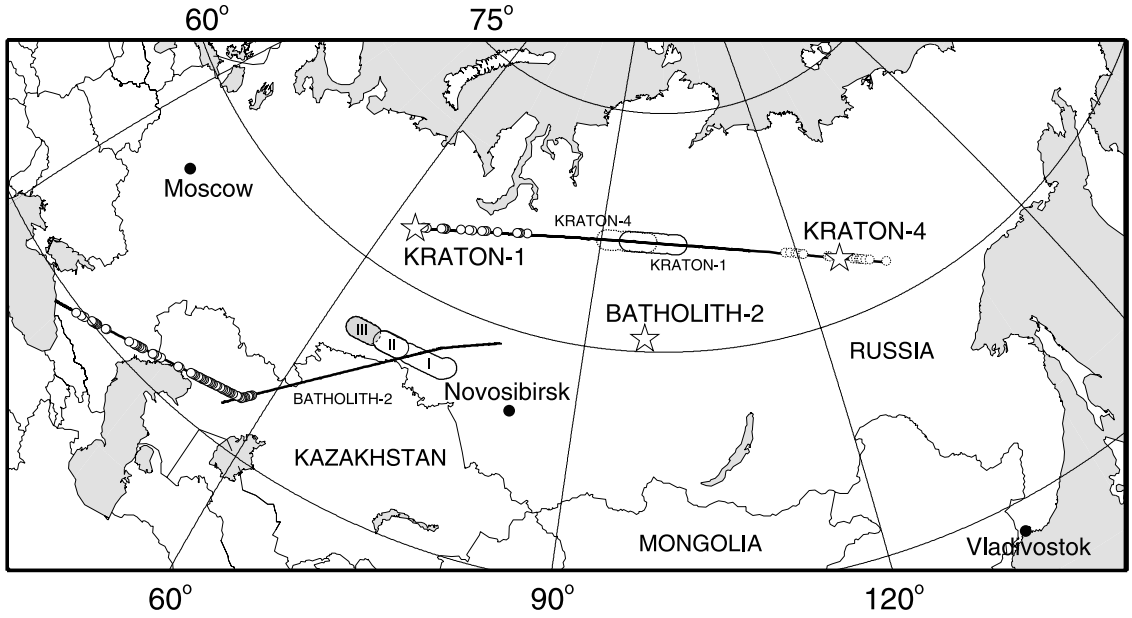

Figure 1. Map of the former Soviet Union showing the location of the two seismic profiles and three PNE shots used in our analysis (Lambert Equal Area projection). The locations of the PNE shots for which we observe seismic signals from the CMB (stars), the trace of the recording station locations (lines), the locations of the individual stations which recorded the *PcP* arrivals (circles), and the locations on the CMB of the bounce points of the observed *PcP* phases (ellipses) are indicated. Roman numerals refer to offset range bins along profile BATHOLITH shown in Figure 3.

insufficient shot-receiver offsets to observe the *PcP* phase, as already mentioned. The KRATON shots had yields of 22 kt (equivalent earthquake magnitude m_b = 5.5 and 5.6 for KRATON-1 and KRATON-4, respectively [*Sultanov et al.*, 1999], and recording station intervals of 10 km, with a maximum source-receiver offset of 3310 km. The other observation of CMB phases is on recordings of the BATHOLITH-2 seismometer array in the region of the Caspian Sea. BATHOLITH-2 had an 8 kt yield (m_b = 5.2) [*Sultanov et al.*, 1999] and was recorded to a maximum offset of 4390 km with Taiga stations.

3. Seismic Observations

[11] The seismic section for KRATON-1 (Figure 2) shows clear first arrivals at almost all offsets with very low levels of noise before the first arrivals on most traces. This is not unexpected given the low levels of cultural noise at the extremely remote locations in which most of the recording seismometers were deployed. The gaps along the profile are the result of noisy traces or lost data not made available to us from the original recordings which had more complete coverage of the offset range. We also have both manually and automatically (by frequency band pass filtering from 1 to 10 Hz) edited noise from the data, primarily to remove large noise spikes, but some traces which contained large amounts of instrument-generated noise have also been removed from the displays of the data in Figure 2. The first *P* arrivals from the mantle (*Pn*) and the transition zone (P_{410} and P_{660}, waves which are refracted below the 410 and 660 upper mantle discontinuities, respectively) are distinct. In addition, reflected arrivals are observed. The *S* arrivals are less distinct and form a region in the seismic section with enhanced energy but no clear arrivals. They are mainly observed at offsets <1500 km. One other arrival on these records is a distinct phase between 200 and 300 s around the maximum offset of the record section corresponding to 525–545 s true two-way travel time. This arrival matches both the arrival time and expected time-versus-distance move-out of a reflection from the core-mantle boundary (*PcP*). The waveform is sharp and distinct on the illustrated scale compared to the long reverberative coda of interfering arrivals following the first arrival in the same offset interval.

[12] This arrival is even more pronounced and stronger on the BATHOLITH-2 section than on the KRATON-1 section (Figure 3). For KRATON-4 the *PcP* arrival is visible but weak. These arrivals can be traced with variable clarity over the offset range 2600–3300 km for KRATON-1, 2500–2900 km for KRATON-4, and 2600–3950 km for BATHOLITH-2 (Figure 3). Hence the arrival is visible on three different PNE recordings, being strongest on the BATHOLITH-2 record. We observe no arrivals from the CMB at offsets smaller than 2200 km (~20°), consistent with global observations of *PcP* [*Astiz et al.*, 1996].

[13] There are no arrivals observed in these data from any boundary in the lower mantle that is not very close to the CMB. Arrivals from D″ have been reported under Siberia from observations on the Gräfenberg array of earthquakes in the Kuril and Aleutian Islands [*Weber*, 1993; *Freybourger et al.*, 1999, 2001]. These authors have suggested the existence of point scatterers in D″ as the cause of the arrivals. The scatterers are located below the Kara Sea several hundred kilometers to the north of the PNE profiles. We do not observe any evidence from the PNE data for arrivals from the top of *D″* or from within *D″* above the ULVZ and the CMB. However, this may be because of the offset

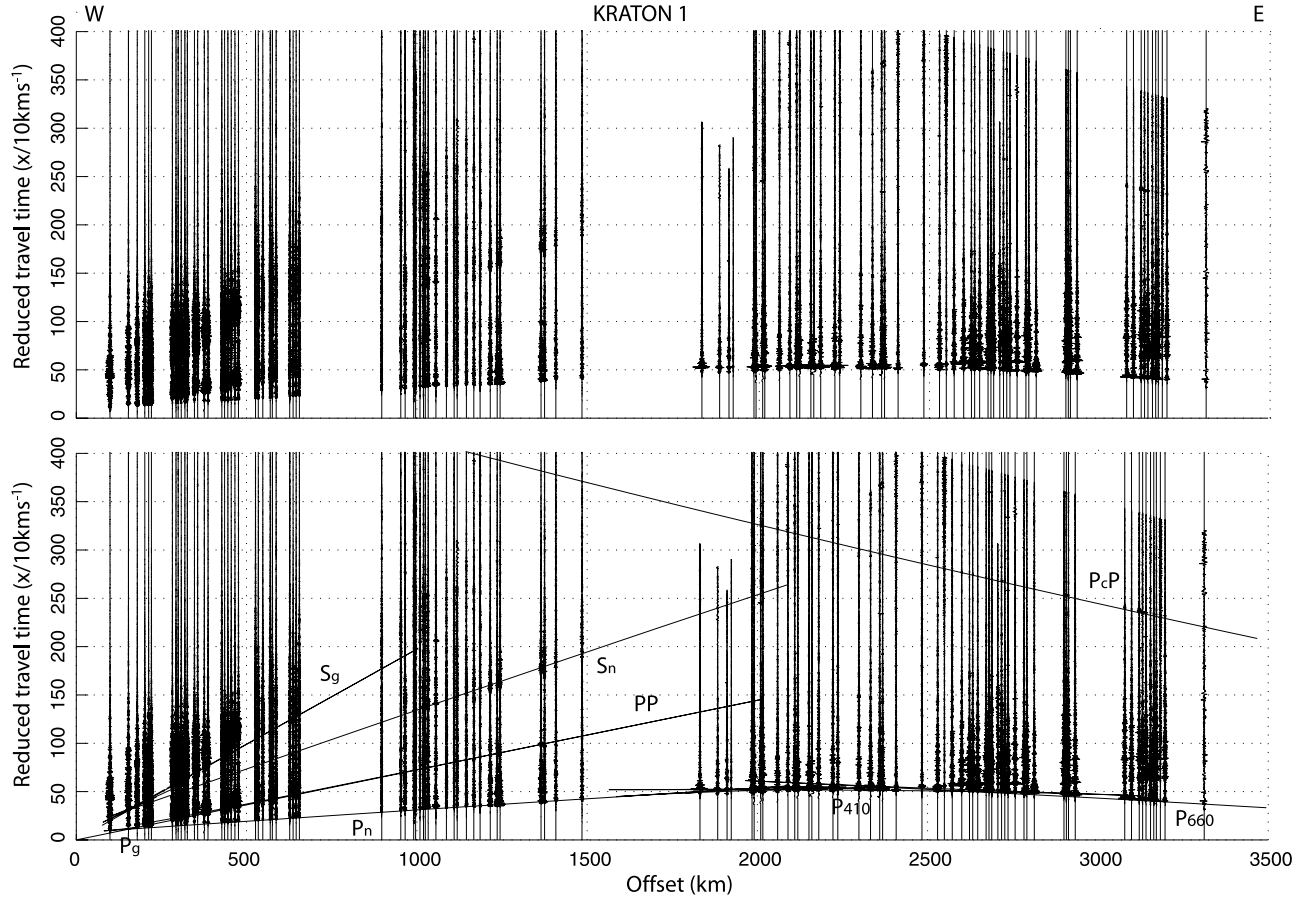

Figure 2. Seismic record section for the KRATON-1 shot recorded to 3400 km offset. (See Figure 1 for shot and profile locations.) The data are displayed with a reduction velocity of 10 km s^{-1}. The expected travel times for *P*, *S*, and *PcP* phases in the IASP91 model [*Kennett and Engdahl*, 1991] are superimposed in the lower plot. The first arrivals correlate with expected travel times for upper mantle arrivals down to the transih *Sg*, *Sn*, and *PP* are also observable. At the far offsets of the profile a strong arrival at 200–300 s after the first arrivals is observed. This phase has an extremely high apparent velocity, and its travel time coincides with a reflected arrival from the CMB (the *PcP* arrival in the IASP91 model). P_g is the direct *P* wave arrival and is the first arrival out to an offset of approximately 150 km. P_n is the *P* wave arrival refracted below the Moho and is the first arrival beyond an offset of 150 km. *PP* is a *P* arrival which has bounced once from the surface before arriving at the recorder. For this data the *pP* arrival is not a distinct phase since the source depth is around 0.5 km.

interval of our observations, and therefore we cannot rule out the possible existence of these scatterers beneath the PNE profiles.

[14] The reflected arrivals from the CMB are observed on both the KRATON-1 and KRATON-4 seismic sections, which are reversed profiles with the two shots recorded on the same array in opposite directions. Consistent travel times and move-out velocities on both of the two reversed sections indicate that this seismic phase originates from beneath the profile and not from out of the profile plane as sideswipe from a shallower boundary at a large distance from the profile. The observation of the same phase for three different shots from two different PNE profiles makes it extremely unlikely that it is some local or source-related artifact which is mimicking an arrival from the CMB. In addition, all these arrivals have the appropriate travel time move-out for *PcP*, making us certain that these arrivals can only be reflections from the CMB.

[15] The first onsets of the CMB arrival on KRATON-1 and KRATON-4 are 0–1 s earlier than the expected travel time for the *PcP* reflection from the core-mantle boundary in the IASP91 model (Figures 3b and 3c). For KRATON-1 the maximum amplitudes of the complex waveforms occur at the expected travel time for *PcP*. On BATHOLITH-2 the onsets are ~1.5 s earlier than the expected *PcP* time between 2800 and 3500 km offset (Figure 3a), with the time difference gradually increasing to 2.5 s at 3800–4000 km offset (Figure 4). These differences could, in principle, reflect relatively high velocity in the mantle or in D'' [*Freybourger et al.*, 1999] but are more likely the result of geometry at the CMB, caused by thickness variation of the ULVZ or possibly by topography of the CMB. These variations would have a wavelength on the order of the variations in travel time residual, i.e., 300–400 km of offset or 150–200 km at the CMB. On all profiles a strong arrival is observed at the expected arrival

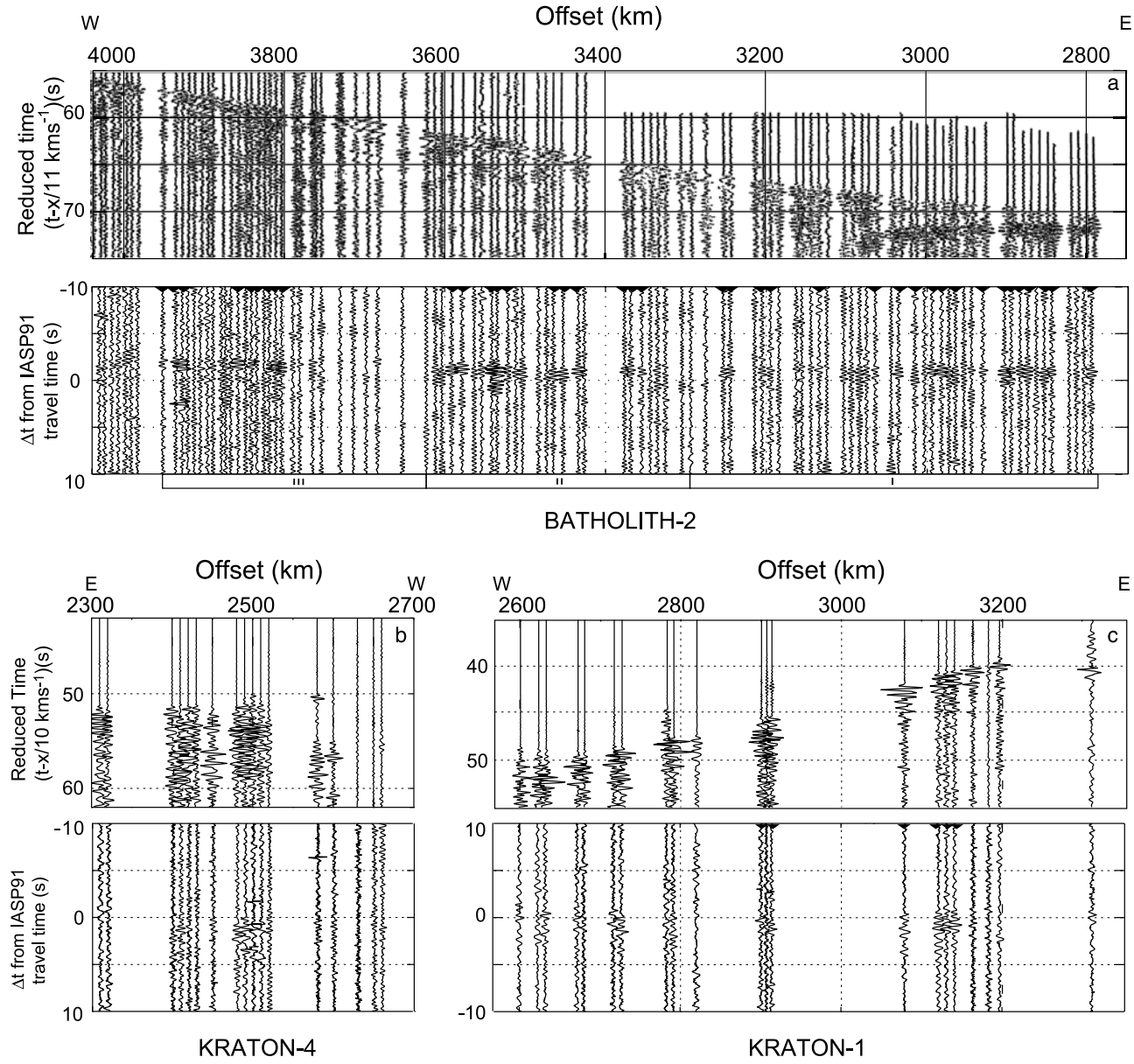

Figure 3. Close-up views of the seismic sections from the (a) BATHOLITH-2, (b) KRATON-4, and (c) KRATON-1 PNE shots for the offset range of 2800–4000, 2300–2700, and 2600–3300 km recorded along the profiles shown in Figure 1. For each of the shots both time windows around the first arrivals and around the CMB arrival are shown. The top panel is displayed in reduced time (reduction velocity 11 km s^{-1} in Figure 3a and 10 km s^{-1} in Figures 3b and 3c). The bottom panel is displayed relative to the expected travel time for *PcP* (calculated using the TauP Seismic Toolkit [*Crotwell et al.*, 1999] and the IASP91 global velocity model [*Kennett and Engdahl*, 1991]). Strong arrivals are observed with onsets 1.5–2 s before $\Delta t = 0$ for BATHOLITH-2, with energy at larger offsets arriving even earlier, up to 2.5 s before *PcP*. For KRATON-1 the onsets are consistently 0–1 s before the expected *PcP* arrival. The early arrivals with long waveforms are consistent with a complex CMB. The traces used for calculation of the waveform stacks shown in Figure 9 (solid triangles) are indicated. The boxes and Roman numerals correspond with the areas labeled in Figure 1 and show the offset bins used to stack the data from BATHOLITH-2.

time for *PcP* after the first arrival from the CMB region, and the arrivals have the appropriate move-out for *PcP*. The ~1 s differences in absolute travel times between the BATHOLITH and KRATON sections probably reflect differences in mantle velocities. The time difference in the first onset on BATHOLITH-2 is 1 s over 1300 km (650 km at the CMB) and varies smoothly along the profile. If this time difference was due to local receiver statics, it should not have such a smooth variation and would vary from trace to trace. The local receiver statics are observed during stacking

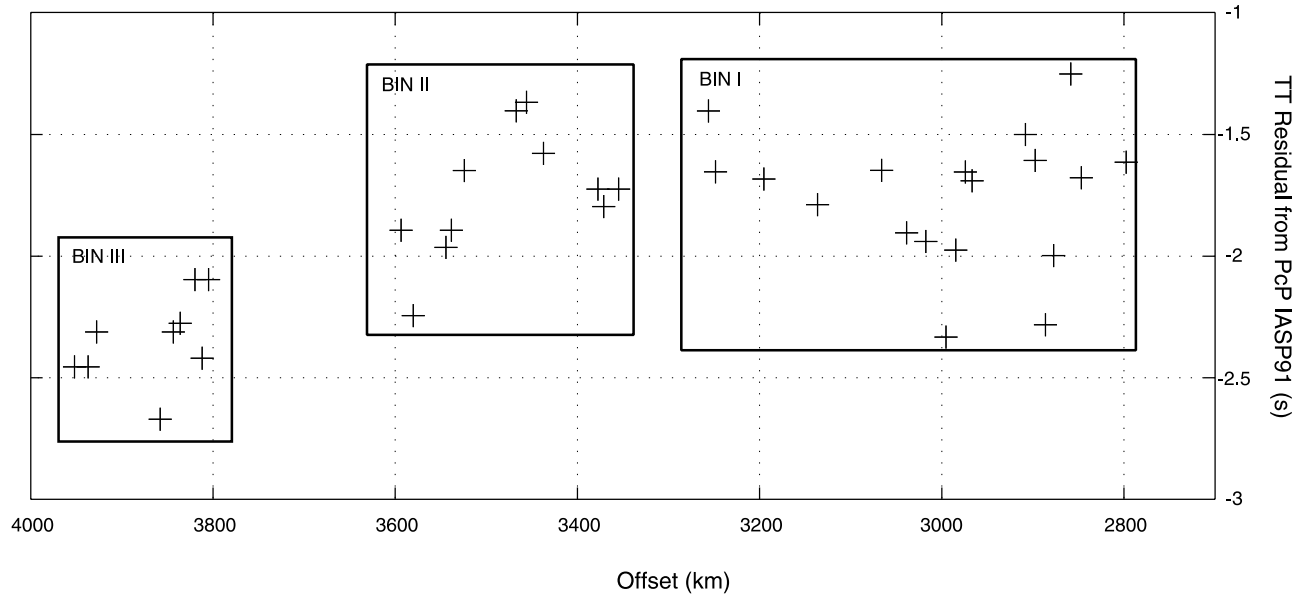

Figure 4. Travel time residuals of the onset of the CMB arrivals from the expected arrival time of *PcP* in the IASP91 model for BATHOLITH-2. The residuals are all negative, showing an early arrival compared to *PcP* and hence either high velocities in the lower mantle or D'' layer [*Freybourger et al.*, 1999] or structure at the CMB in this region. The residuals can be grouped into three bins with distinct differences in travel time residual. Variations in mantle velocity structure cannot be ruled out, but given the relative wavelengths of the arrival time variation and likely mantle velocity variations [*van der Voo et al.*, 1999], it is more likely that they result from variations in velocity structure at the CMB. The bins located in Figure 1 and indicated on the data in Figure 3 are shown (boxes). These bins provide the data for the stacks labeled with the same Roman numerals in Figure 9.

of the data. They are only on the order of a few hundred milliseconds.

4. Instrument Responses

[16] Analogue short-period, Taiga-type instruments were used to record most Soviet PNEs. These are ground displacement recorders and were deployed over large distances in typically very rough terrain with very poor access. The instrument response of the Taiga seismographs has been measured for several of the instruments, and the result was provided to this study for each of these instruments. These reference signals, A_r, are included at the end of the traces for several stations for each PNE profile in the distributed data made available from Russia. This information is not included for all stations, however. The amplitude response varies with frequency up to a sharp drop-off from 10.5 to 12 Hz (Figure 5). For an unknown reason the seismographs were set to a different response for offsets from 0 to 495 km and over 500 km. The ground displacement (L) in nanometers is given as

$$L = \frac{AE}{A_r K}, \tag{1}$$

where A is the seismic signal amplitude recorded by the seismograph, A_r is the reference signal amplitude, K is a geophone parameter in μV nm^{-1}, and E is a reference parameter in μV with two different functions versus frequency for offsets of 0–495 km and for more than 500 km. These parameters were all measured for a seismic signal of dominant frequency F between 0 and 10 Hz. The reference signal A_r (Figure 5a) has high amplitude at high frequencies, as do both the parameters K and E (Figure 5c). This results in a relative amplification of high frequencies by the Taiga seismographs up to a maximum frequency cutoff at 10.5 Hz, followed by a very sharp drop-off (Figure 5b). Therefore the seismograph acts as a high-pass filter on the data (Figure 5d). The instrument response differs significantly from the instrument response of other short-period seismometers which have recorded the arrivals from PNE shots (Figure 5b). In addition to the instrument response discussed here, most of the PNE data were filtered after recording with a low-pass frequency filter with a frequency cutoff at 10 Hz. The original unfiltered data are not available for almost all the PNE data. The one exception is the QUARTZ PNE profile on which we have been unable to identify any CMB phases. We find that the frequency response of the seismic instruments as provided by our Russian colleagues is correct, as demonstrated by deconvolution of the recorded signals at certain offsets, which leads to similar waveforms as recorded on Gräfenberg and NORSAR at the same offsets (Figure 6b).

5. First Arrivals

[17] A simple test of the significance of the *PcP* arrivals on KRATON-1 with regard to CMB structure is the relative length of the *PcP* arrivals to the direct arrivals. This comparison is complicated by the existence of several

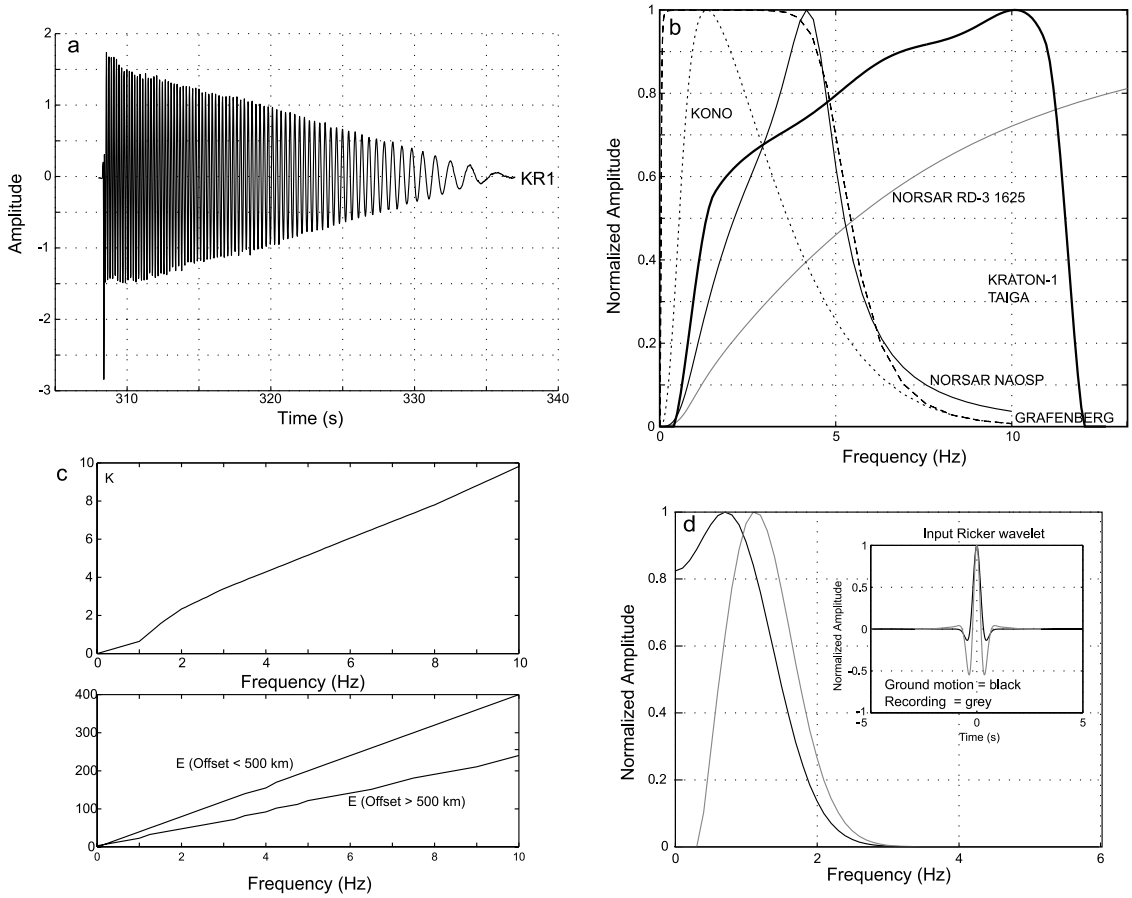

Figure 5. Measured instrument response and theoretical response parameters for the Taiga seismometers used in recording Russian PNE data. (a) Calibration pulse (recorded at the end of a number of individual traces on the PNE records) showing increasing amplitude with frequency. (b) Calibration pulse with a drop-off in sensitivity beyond 10.5 Hz in the power spectrum. Frequency responses (amplitude spectra) for selected short-period instruments from NORSAR, station KONO (part of the Global Seismic Network), and the Gräfenberg array are shown for comparison. The Taiga seismometer has a higher sensitivity than most short-period recorders at frequencies above 5 Hz. In order to estimate an average instrument response, we fit a polynomial function to the average of several of the frequency responses. Only a few stations have response information forcing us to estimate responses for the other instruments from those we have. Fortunately, these individual responses show a large degree of similarity. (c) Two other parameters, K and E, determining the frequency response of the PNE instruments. These parameters effectively show a linear amplitude increase with frequency. The frequency response is a combination of these parameters and the calibration pulse (equation (1) in text). (d) Applying the Taiga frequency response to a theoretical waveform with a peak frequency of 1 Hz, which results in a shift to high frequencies in the power spectrum.

branches from transition zone structure in the offset range where the PNE data show arrivals from the CMB. However, if the length of the direct *P* arrival and *PcP* are the same, then there is nothing to suggest that additional structure exists at the CMB. However, the existence of fine structure at the CMB would be suggested if there is a significant difference in the character. If the *PcP* arrival is longer then the direct wave, this would clearly show CMB structure.

[18] An example of the KRATON-1 first arrival recorded at 3430 km on the Gräfenberg array station GRB2 shows a simple first arrival (Figure 6). The first arrivals from KRATON-1 at the NORSAR array and on the PNE sections are more complex because there are three interfering *P* branches at this offset (2620–2680 km) (Figure 6). The first arrival on the Gräfenberg record is similar to the short-offset arrival recorded with Taiga instruments, i.e., the *Pn* arrival in the offset interval 180–350 km (Figure 7a). At other offset ranges the first arrivals are the complex interference of several reflected and refracted arrivals from the upper mantle and transition zone making the determination of the direct waveform impossible from the first arrivals. In the appropriate offset range the first *P* is a combination of at least three different arrival branches from the transition zone (Figure 7b). Hence our observations of CMB phases are in the same offset interval as the complex interference phases from the transition zone. Therefore we cannot compare the CMB arrivals to the first arrival waveforms at the same offset to assess the complexity of the CMB structure.

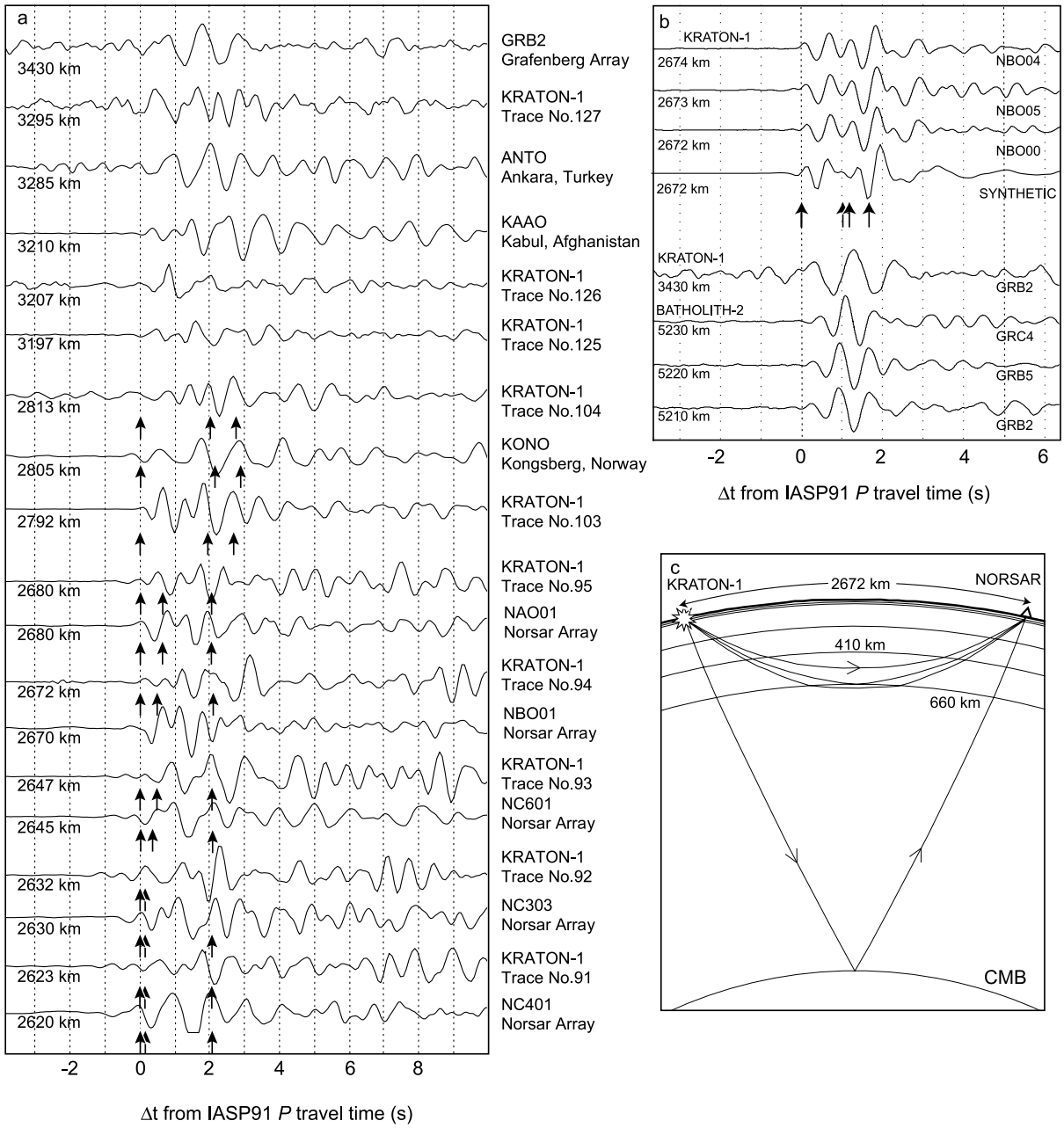

Figure 6. (a) First arrivals for KRATON-1 recordings compared to data from the NORSAR array, Gräfenberg array, and other seismic stations with short-period seismographs. The offsets and data sources are indicated next to the traces. All data are displayed relative to the theoretical *P* arrival time from the IASP91 standard model. Theoretical *P* arrivals from the upper mantle and transition zone (arrows) are indicated. For nearly every case, there is more than one *P* arrival branch which complicates the first arrivals significantly because of interference between the phases. The first arrivals are much simpler for large offsets where only one *P* arrival is expected, mainly because of the lack of interfering phases as seen on the trace from the Gräfenberg array at 3430 km offset. (b) First arrivals for KRATON-1 and BATHOLITH-2 for short-period recording arrays outside the former Soviet Union. Arrows indicate *P* arrival times at the NORSAR data for KRATON-1 (station codes beginning with NB, top 3 traces). These arrivals are more complicated than for the same shot recorded by the Gräfenberg array at larger offset (station codes beginning with GR), which show a simple arrival for both KRATON-1 and for BATHOLITH-2 at even larger offsets (last 3 traces). For comparison, the synthetic seismogram at offset 2672 km is shown convolved with the instrument response of the NORSAR array. (c) This synthetic seismogram calculated for the IASP91 model [*Kennett and Engdahl*, 1991] and modified to include a seismic interface at 538 km and the 660 km interface shifted to a depth of 662 km. Ray paths for *P* and *PcP* arrivals from KRATON-1 to the NORSAR array, showing the multiple arrivals from the transition zone at a source-receiver offset of 2672 km, are shown.

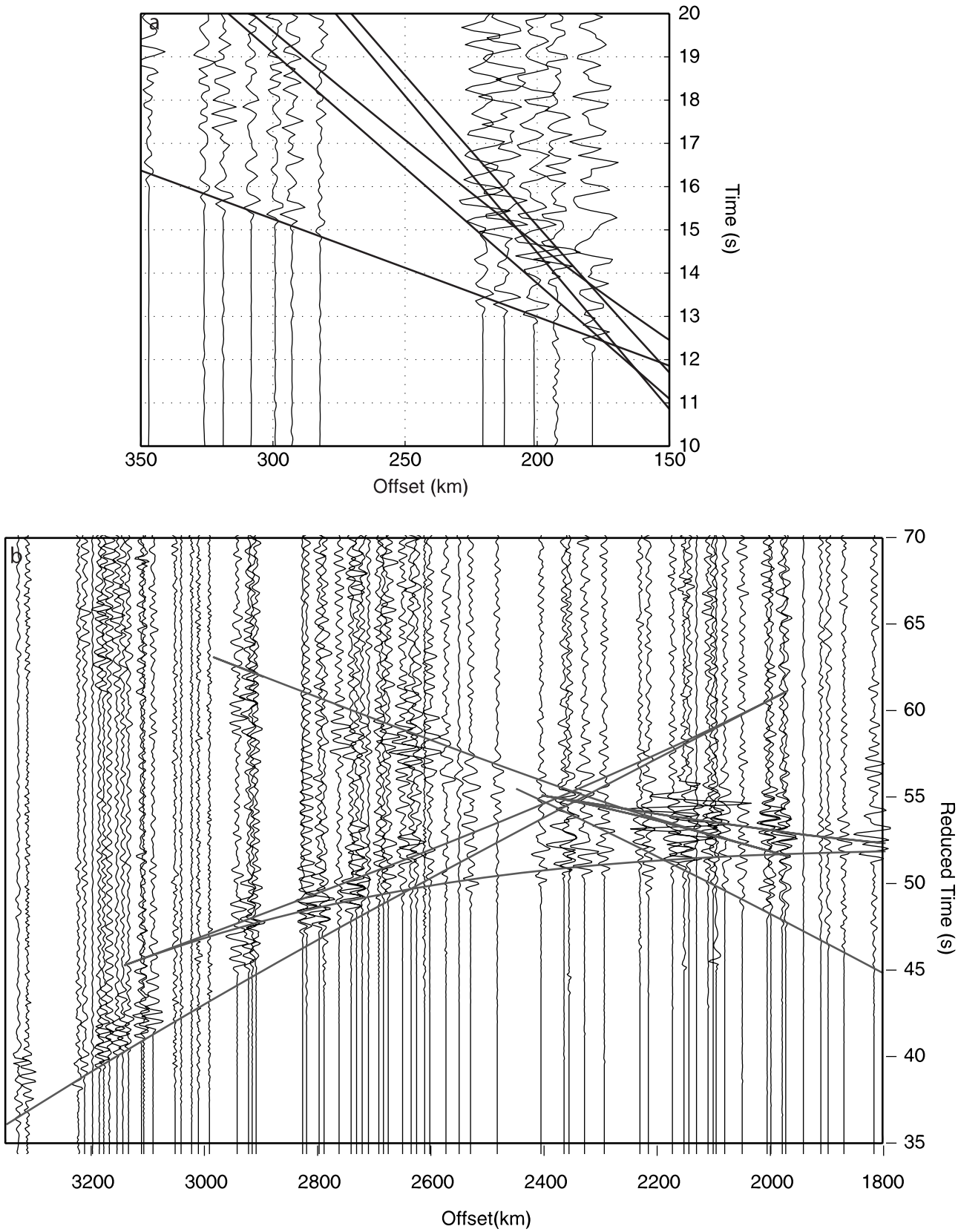
a
20
19
18
17
16
15
14
13
12
11
10
Time (s)
350
300
250
200
150
Offset (km)
b
70
65
60
55
50
45
40
35
Reduced Time (s)
3200
3000
2800
2600
2400
2200
2000
1800
Offset(km)

Figure 7

Instead, we estimate the source waveform from near-source and very long-offset recordings (e.g., Gräfenberg) for this evaluation.

[19] It has been suggested that the long-lasting first arrivals observed at the offsets where we see the CMB arrivals may be caused by source effects. One possibility is that the complex waveform is caused by ghosts from the free surface. However, the depth of the detonations was between 0.5 and 1 km, which corresponds to a delay time for the ghost of <0.5 s. This is much shorter than the observed length of the CMB phases. It has been proposed that the long direct waveform at these offsets is due to spalling and the collapse of the cavity produced by the exceptionally large charges. However, synthetic modeling of PNE source characteristics using local geological models obtained from borehole logs reproduces the observed waveforms without introducing spall or collapse effects [*Murphy et al.*, 2001]. We find that such effects are mainly observed on recordings of waves from the nuclear explosion test sites, such as at Semipalatinsk and Novya Zemlya. Furthermore, the observed first arrivals at short offsets (*Pn* arrivals at 180–330 km) and at far offsets (>3500 km) are simple and show no indication of trailing energy to the main direct phase (Figure 7). Hence such effects can be ruled out as possible causes of the long direct waveform. In many cases the first arrival is substantially longer than the CMB phases which clearly demonstrate that its length may be determined by interference between several seismic phases.

[20] The waveform of the first arrivals is the combined interference effect of several waves that arrive from the mantle transition zone. Therefore we cannot use first arrivals on the traces that recorded the *PcP* reflections as input waveforms for modeling. Instead, we estimate the source waveform from the small offset recordings of the *Pn* wave signal where there is least contamination from upper mantle structure. This approach is justified by a simple first arrival from the KRATON-1 shot recorded at the Gräfenberg array (Figure 6). NORSAR and Gräfenberg array data show simple first arrival waveforms from PNEs except at medium range offsets (around 2000–3200 km) where multiple branches produce multiple first arrivals. Data from other stations show similar variability (Figure 8).

[21] The difference in length of the *PcP* arrivals indicates that there is a difference in the character of the interfaces which produce the arrival. The long waveform of the CMB arrival is not consistent with a reflection from a simple first-degree discontinuity between the lower mantle and the outer core. Hence these arrivals suggest additional structure at the CMB which we can observe in the *PcP* arrival. In section 6 we discuss stacking of the data and variations in the resulting waveform from different offset bins. This provides further indication that there is additional complexity at the core-mantle boundary. If all complexity in the *PcP* arrival was due to source or receiver effects, these effects should be either universal (for source effects) or most likely at short wavelength and random. The fact that we can identify groups of arrivals with common characteristics which include 10–20 different traces and hence an offset range of l00–200 km is neither random nor universal. It is a result of complexity at or around the CMB.

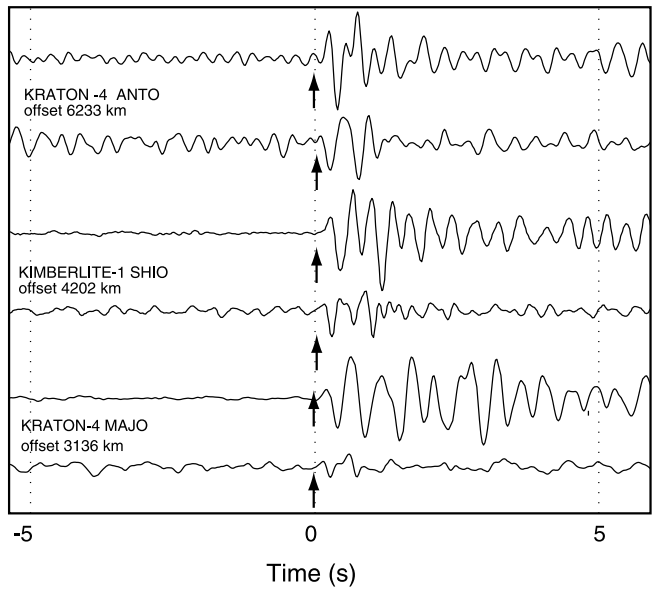

Figure 8. Seismograms for the two PNE shots KRATON-4 and KIMBERLITE-l shown in a window around the first arrivals and phases from the CMB. The length of the first arrivals is highly offset-dependent, whereas the *PcP* waveform is more constant. These traces were recorded by short-period seismographs outside of the former Soviet Union. For the shortest-offset case the *P* and *PcP* arrivals are dissimilar with different durations. However, the duration and waveform of the arrivals tend to become similar with increasing offset. Seismic stations are as follows: MAJO is Matsushiro, Japan; ANTO is Ankara, Turkey; and SHIO is Shillong, India.

6. Data Stacks and Lateral Variation in *PcP*

[22] The data quality is high enough for KRATON-1 and BATHOLITH-2 to estimate the signal waveform at certain offsets on single seismograms. As a result of the large number of traces we can further improve the signal-to-noise ratio by stacking the data. This allows a good estimation of the exact shape of the waveform at the CMB. The overall length of the arrivals is typically 2–3 s, which is significantly longer than expected from reflectivity calculation of the reflection waveform for a single interface using the IASP9l model and an average wavelet derived

Figure 7. Details of record sections for KRATON-1 (trace normalized). (a) First arrivals (*Pn*) in the offset range 150–350 km. These arrivals are simple. (b) First arrivals in the offset range 1800–3500 km (where *PcP* arrivals are observed at later travel times), showing a complicated interference of arrivals from the upper mantle and the transition zone. Theoretical travel times for *P* arrivals from the IASP91 model (straight lines) are shown. At most offsets within this range the first arrivals are a combination of several branches. Additionally, we expect reflections from an interface at ~520 km depth [*Ryberg and Wenzel*, 1999], for which the travel times are not shown.

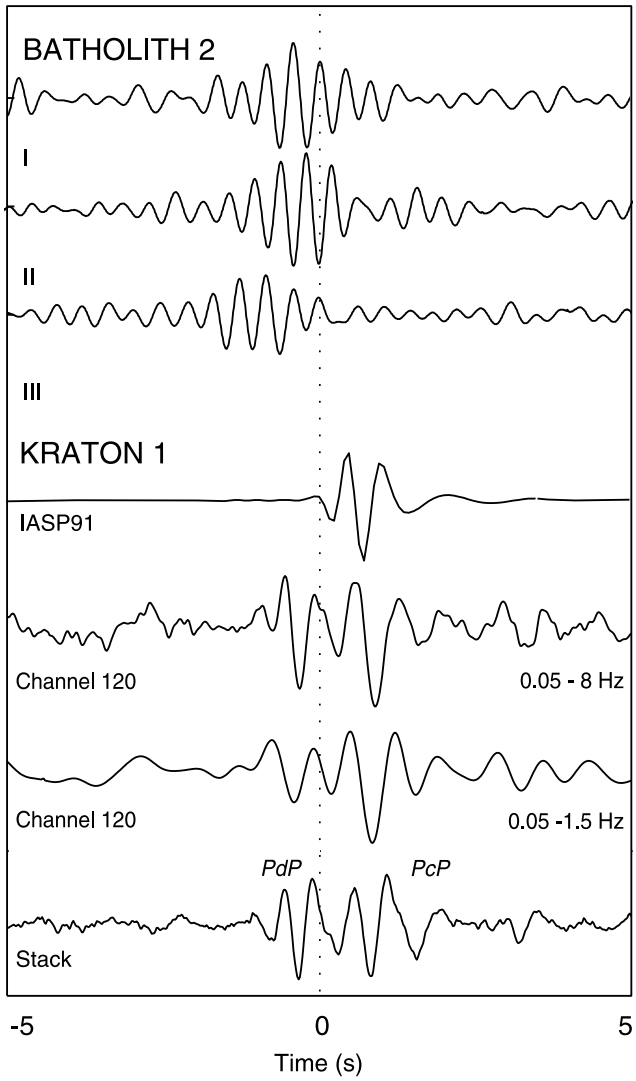

Figure 9. Waveforms of the KRATON-1 and BATHOLITH-2 core-mantle boundary arrivals and the calculated waveform for a reflection from a single interface CMB, assuming propagation through the IASP91 velocity model. The data show two separate phases (*PdP* and *PcP*). Most traces are stacked. To take into account local receiver statics and difficulties with picking the onset of the CMB arrivals for some traces, maximum power stacks were calculated for one offset bin for KRATON-1 and for three offset bins for BATHOLITH-2. Only the traces indicated by triangles in Figure 3 were used for stacking. However, adding the other traces makes no difference to the overall waveform shape and length. Numerals refer to offset bins located in Figure 1 and indicated in Figure 3. There are clear differences in the waveform and complexity of the stacks for each offset bin. The source waveform for modeling the KRATON-1 stack was extracted from a windowed stack of direct arrivals in the offset range 180–300 km (compare to Figure 7a). The change in amplitude of *PdP* with frequency is identifiable on individual traces (channel 120 from KRATON-1 is shown here as an example). A significant amplitude reduction for *PdP* occurs when frequencies above 1.5 Hz are removed but not for the *PcP* arrival. Time is measured relative to the predicted arrival time of *PcP* according to the IASP91 model.

from the near-source arrivals from KRATON-1 (Figure 9). No near-offset arrivals were recorded for BATHOLITH-2, but the source parameters of the two PNEs are likely to be similar where the frequency content may be slightly higher for the BATHOLITH shot than the KRATON shot (Figure 6b). Application of a Hilbert transform to the digital BATHOLITH-2 data produces a waveform which closely matches the waveform estimate for KRATON-1. The higher frequency content for arrivals from the BATHOLITH-2 shot than the KRATON shots is a source-related effect, as evident from a comparison of the arrivals from these two shots on the Gräfenberg and NORSAR arrays (Figure 6b).

[23] We interpret the recorded waveforms from around the CMB as a combination of at least two separate arrivals: (1) from the top of the ULVZ (*PdP* [*Revenaugh and Meyer*, 1997]) and (2) from the CMB (*PcP*) with possible other reflections in between. These are the first data to show the existence of the ULVZ at the CMB in Siberia [*Garnero et al.*, 1998]. The complex waveform cannot be caused by near-surface reverberations, since they are unlikely to affect all stations over an 800–1200 km range of offsets. Further, the recordings of the KRATON-2 and KRATON-3 shots show simple waveforms comparable to the *Pn* arrival for KRATON-1 and KRATON-4 in near offset on the same stations that show the complex CMB waveforms for KRATON-1 and KRATON-4. If the long waveform of arrivals from the CMB had been the effect of crustal structure, *Pn* would have been a long, reverbatory arrival on the same stations for KRATON-2 and KRATON-3. Surface ghosts (*pP*) for the PNE source depths (593 m for KRATON-1, 567 m for KRATON-4, and 720 m for BATHOLITH-2) are too close to the direct pulse to explain the long wave train and also result in additional complexity of the first arrival. Other source-related effects such as delayed collapse of the cavity produced by the shot can also be disregarded because both recordings of *Pn* at short offset and the first arrival at long offset (>3400 km) show very simple waveforms; compare to the recording of KRATON-1 on the Gräfenberg array (Figure 6).

[24] Close examination of the arrivals from KRATON-1 and BATHOLITH-2 shows variation between individual traces. On the BATHOLITH-2 record section the variation between the traces is less than for KRATON-1, but BATHOLITH-2 has a systematic variation along the record (Figure 3). Three offset ranges appear to have relatively coherent waveforms which vary in absolute travel times and waveform duration (Figures 3 and 4). These variations are likely due to variations in the properties of the CMB along the BATHOLITH-2 profile. The lateral variation in the waveform indicates lateral variation in the properties (thickness or velocity) of the ULVZ with a wavelength of 150–200 km at the CMB. The short arrival in stacking bin III (Figure 3) indicates a region where there is a much thinner, or nonexistent, ULVZ than in the other two bins. These are most likely small variations in thickness.

[25] The impression provided by the raw data is confirmed by the data stacks (Figure 9). The data were stacked by aligning the arrivals within each stacking bin (three bins for BATHOLITH-2 and one bin for KRATON-1) such that the first onset time of the CMB arrival was the same. The validity of the resulting stacks was checked by randomly moving traces relative to each other to discover if any bias

was applied in picking the first arrivals. The very large travel time difference between the first arrivals and the CMB arrivals as well as their different travel paths in the mantle means that variations in arrival time from the expected arrival time for the first arrivals (receiver statics) do not necessarily correspond in detail to the variations apparent in the CMB arrivals. Therefore the first arrival statics are not a good guide for stacking the CMB arrival, although variations in the stacks appear to be similar to those observed in the first arrivals.

[26] One concern in estimating variability at the CMB is the large size of the Fresnel zone and therefore the low resolution of short-wavelength features at the CMB in our data. The size of the Fresnel zone for 1 Hz at the CMB is 130 by 260 km [*Weber*, 1993]. The frequency content of the signals is much higher for PNEs than for earthquakes, such that the Fresnel Zone is considerably smaller for these data, on the order of 50 by 80 km. Our profiles are long enough to sample the CMB over more than one Fresnel zone, and therefore we do have information about lateral variation at the CMB. In contrast, data recorded at the NORSAR and Gräfenberg arrays have bounce points within one Fresnel zone so that any lateral variation within these arrays is probably caused by local structure at the receivers and cannot be related to structure at the core-mantle boundary.

[27] The BATHOLITH-2 record section shows variation in absolute arrival time over its offset range. Both core-mantle boundary topography and mantle velocity variations can cause changes in the absolute travel time of arrivals from the core-mantle boundary and will cause variations in the arrival time with a wavelength that corresponds to the wavelength of the velocity or topography variations. Variations in travel time might be due to interference of phases from the CMB where the ULVZ may decrease the amplitude of the first part of the arrival (*PdP*) and preserve the second part (*PcP*), which will create a short, apparently delayed arrival.

[28] We have compiled some short-period recordings from both the PNEs and other Soviet nuclear explosions, i.e., weapon tests from Semipalatinsk (in what is now Kazakhstan) and Novya Zemlya (Figure 10). The compilation illustrates the large variability in waveform of the CMB arrivals with offset and azimuth. For the Chiang Mai (CHTO) station the first arrival and CMB waveforms are similarly indicative of a simple CMB. The data from the Ankara station (ANTO) show a double reflection for the CMB region at far offsets indicative of a well-developed ULVZ, also here with a tendency for a high-frequency precursor compared to the second arrival. This station also illustrates how a complex first arrival may be measured in front of a double CMB arrival with much shorter duration (at 1515 km offset) similar to our observations on the PNE data at offsets out to ~3200 km. The Toledo (TOL) station shows a relatively complex first arrival and generally a more complex CMB wave train with substantial offset-dependent variation. Waveforms at individual recording stations from different tests fired in close proximity (e.g., at the Novya Zemlya test site) show significant similarity over long time periods (Figure 11a). At some offsets the amplitudes of the *PcP* arrivals and the primary *P* are similar; in particular, at offsets close to 4500 km (Figures 11b and 11c). The lateral variations in

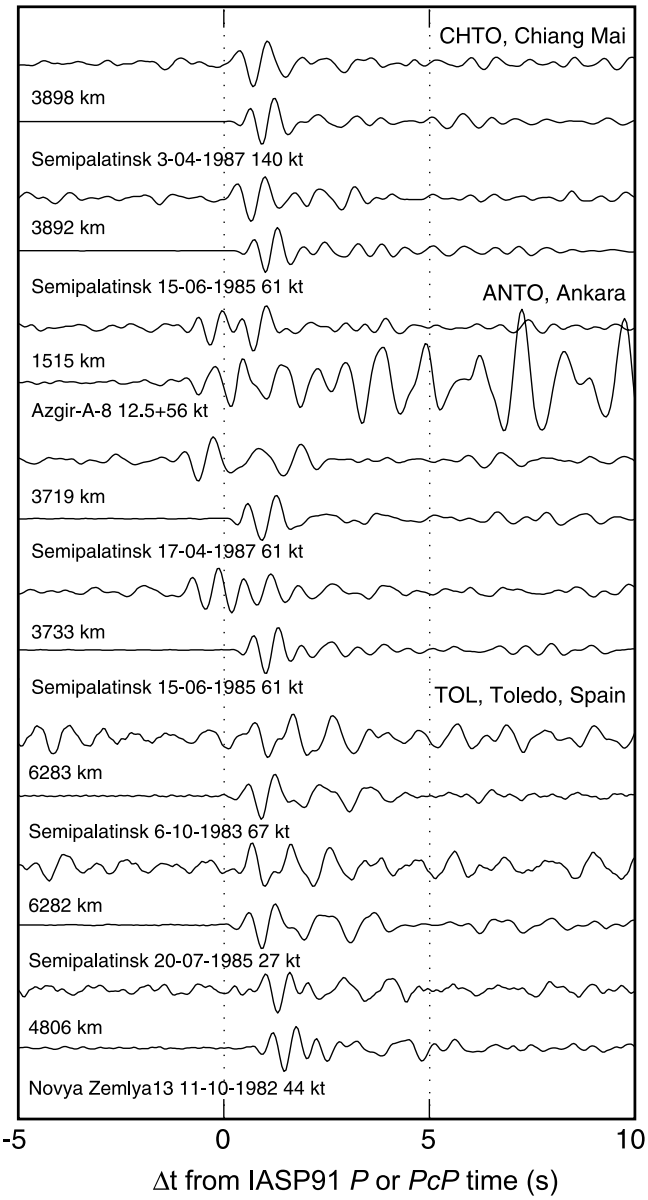

Figure 10. Records of first *P* and *PcP* arrivals for different seismological stations and nuclear test shots. The waveform of *PcP* resembles the first arrival for station CHTO, whereas the *PcP* arrival is much more complex and of longer duration than the first arrival for station ANTO, even though the first *P* is very similar for both stations. At shorter offset, station ANTO shows a very complicated first *P* but only a slightly longer and more complex *PcP* waveform. The recordings at station TOL are similar for *P* and *PcP* for test explosions at Semipalatinsk. These records indicate the existence of an ULVZ at the bounce point of the ray on the CMB. Records of a test shot at Novya Zemlya at the same station show almost similar waveforms for *P* and *PcP*, indicating a simple CMB at this bounce point.

PcP character suggest a large degree of variability in the nature of the CMB under Siberia. The amplitude of the *PcP* arrivals from the PNE shots is very high at offsets of 4000–5000 km for a number of azimuths in agreement

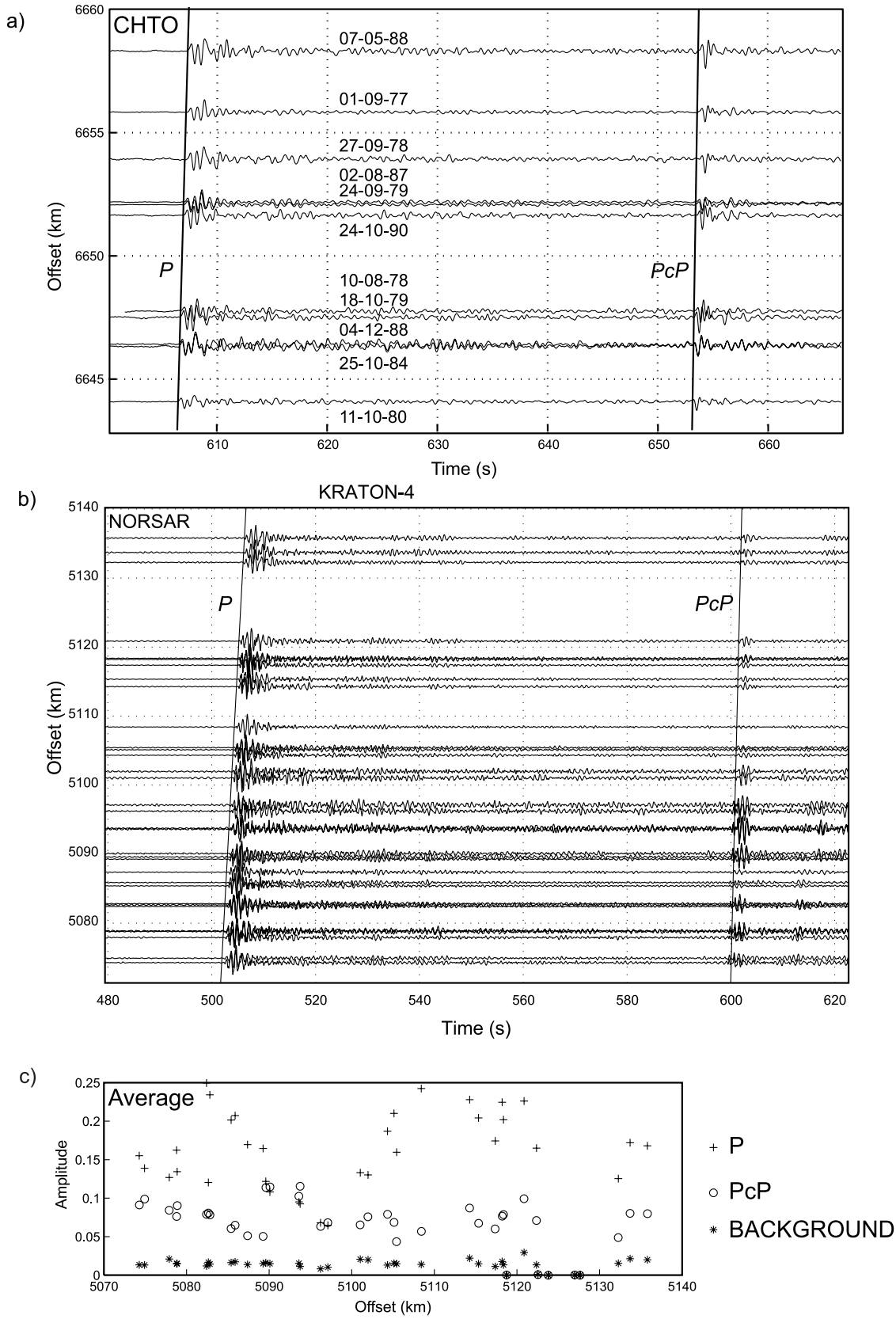
a)
CHTO
07-05-88
01-09-77
27-09-78
02-08-87
24-09-79
24-10-90
10-08-78
18-10-79
04-12-88
25-10-84
11-10-80
P
PcP
Offset (km)
Time (s)
b)
KRATON-4
NORSAR
P
PcP
Offset (km)
Time (s)
c)
Average
Amplitude
Offset (km)
P
PcP
BACKGROUND

Figure 11

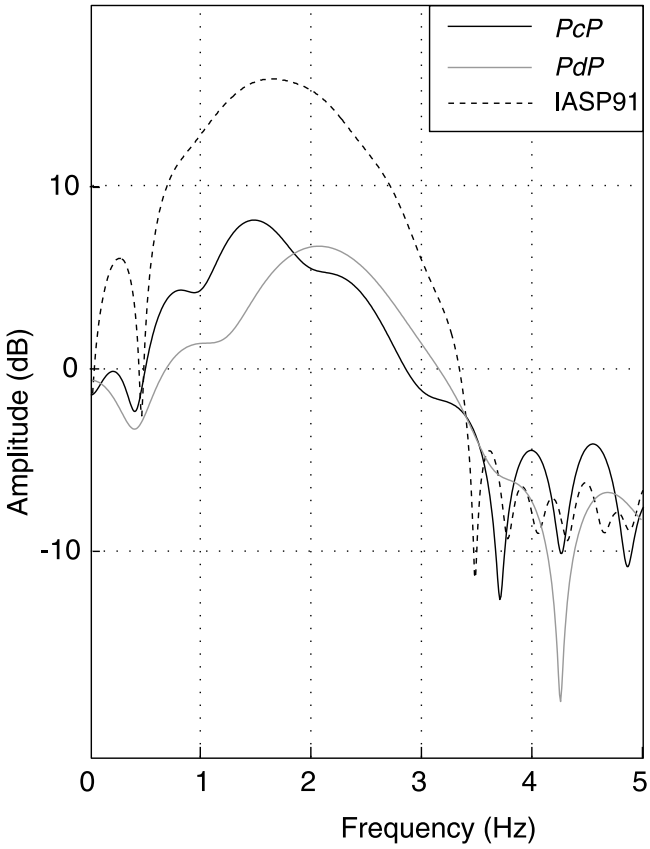

Figure 12. Amplitude spectrum for the KRATON-1 stacked *PdP* and *PcP* arrivals together with the calculated reflection from a single CMB interface in the IASP91 model. The window size is 2 s for each spectrum with a cosine taper applied at both ends of the data window. Note that the *PdP* phase has a significantly higher frequency content than the *PcP*, with a peak amplitude at 2.2 Hz as opposed to 1.5 Hz. The calculated arrival has a peak frequency close to that of the *PcP* phase.

with the expected variation in reflection coefficient for *PcP* from modeling [*Kampfmann and Mueller*, 1989].

7. Frequency Split

[29] For the KRATON-1 shot the stacked waveform has two interesting features. First, amplitudes are above the ambient noise level at frequencies up to 3.5 Hz with the peak frequency being 0.7 Hz higher for the early (*PdP* = 2.2 Hz) than for the late (*PcP* = 1.5 Hz) phase (Figures 9 and 12). Second, the amplitude of the precursor (*PdP*) is close to that of the main arrival (*PcP*). Typical earthquake recordings show significantly lower amplitudes of *PdP* than *PcP* and require stacking of data to resolve the *PdP* phase [*Mori and Helmberger*, 1995; *Revenaugh and Meyer*, 1997; *Williams et al.*, 1998]. In the PNE data the *PcP* and *PdP* phases are visible without any processing (Figures 9 and 3). Application of an appropriate low-pass frequency filter (at 1.5–2 Hz roll-off) to the KRATON data significantly reduces the amplitude of the *PdP* phase relative to the *PcP* phase (Figure 9) and makes the trace appear similar to other observations based on earthquake data at low frequency. The preferential reflection of high frequencies suggests tuning within a thin layer at the top of the ULVZ [*Ake and Sanford*, 1988]. We investigate this possibility by applying reflectivity modeling to the core-mantle boundary reflections.

8. Modeling

[30] A simple calculation of travel time versus offset based on the IASP91 Earth model confirms that the observed arrivals in the PNE data are from the CMB. We have also demonstrated that the waveforms are too long to be simple, first-order reflections from the CMB. In this section we discuss modeling with the aim of investigating the possible range of fine structure at the CMB which could lead to the observed arrivals.

[31] We modeled the stack from KRATON-1 using the reflectivity program [*Fuchs and Mueller*, 1971] based on one-dimensional models of the spherical Earth. We fit four main observations: (1) the separate *PcP* and *PdP* phases, (2) the overall duration of the wave train, (3) the high amplitude of *PdP* relative to *PcP*, and (4) the different frequency content of the two phases (Figure 12). The variables are the number of layers, the layer thicknesses, the layer *P* wave velocities, the layer *S* wave velocities, the layer densities, the velocities and densities in the lowermost mantle, and the outer core and the attenuation in the layers at the boundary. The wide range of variables makes the modeling necessarily nonunique. Furthermore, we have only a limited amount of data to model since we lack access to the first arrivals from BATHOLITH-2. Hence the model we produce only applies to a limited region of the CMB.

[32] The input waveform was extracted from first arrivals on near-offset traces between 200 and 350 km offset, i.e., *Pn* arrivals. This is a simple waveform (Figure 7a). Our choice of input waveform is justified by recordings from long offsets (>4000 km) where a simple first arrival is also observed (Figure 6b). Intermediate offsets have more complicated first arrivals because of the multiple arrivals from the mantle transition zone which interfere at these offsets

Figure 11. (a) Records from several explosions at the Novya Zemlya test site recorded at station CHTO (Chiang Mai, Thailand). The explosions had magnitudes of between 5.6 and 5.9 m_b. They have very impulsive *P* onsets and clear *PcP* arrivals. The *P* and *PcP* arrivals from different nuclear tests show a great deal of similarity even though the shots range in time from years 1978 to 1990. There is no precursor to *PcP*, indicating a simple CMB boundary at this location, and the first arrival waveform is more complex than the *PcP* arrival in this offset range. (b) Recording of the KRATON-4 PNE by the NORSAR array. A very clear *PcP* arrival is present at almost all stations of the array. (c) The amplitude of this arrival relative to the first arrival, plotted as mean amplitude in a 15 s window around expected arrival time. For some stations the *PcP* arrival amplitude equals the *P* arrival amplitude. The noise level was calculated in a window beginning 20 s before the *PcP* arrival.

and so cannot be used. This is the case for the offset ranges where CMB phases are observed. The synthetic trace calculated at 2672 km offset for our input waveform resembles closely the recorded signal on the NORSAR array (Figure 6b). The waveform has been filtered with the instrument response of the NORSAR recorder.

[33] The simplest modeling case is a single interface between two half-spaces with the velocities and densities according to the IASP91 model. Modeling the *PcP* arrival with this simple model does not lead to the observed waveform complexity. Rather, the calculated waveform is very simple with too short a duration to explain the observations (Figure 13a). The simple *PcP* reflection cannot explain the observations, which leads us to investigate a more complicated set of boundaries at the CMB.

[34] The second simplest possibility is a one-layer model of the CMB defined by two interfaces. We investigated this initially with a range of models with both positive and negative velocity contrasts relative to the lower mantle velocity. A high-velocity/high-density layer produces a set of models which do not resemble the expected waveform in any way when constrained to the overall waveform length observed. However, a velocity decrease produces a much more acceptable waveform, particularly with respect to the relative polarity of the two separate arrivals. Varying the thickness of the layer (Figure 13a) shows that a more than 10 km thick layer produces too long a waveform while a 5 km thick layer produces too short a waveform. There is a trade-off between layer thickness and velocity (in this case we assumed a velocity of 12.3 km s^{-1} corresponding to a 10% velocity decrease from the lower mantle velocity of 13.6 km s^{-1}). A different velocity would produce a different thickness. The maximum and minimum velocities (and thicknesses) are limited by the lower mantle and outer core *P* wave velocities, respectively. These constraints fix the maximum thickness at 8.2 km and the minimum thickness at 4.8 km in a simple ULVZ model.

[35] Since neither a single interface at the CMB nor a simple one-layer ULVZ can explain the observed waveform, we have to include yet further complexity at the CMB. A two-layer model matches the waveform and reproduces the observed frequency difference between the two parts of the waveform by tuning in the thin upper sublayer (tuned to frequencies at 2.5 Hz for the *PdP)*. A high-velocity lower layer produces the wrong polarity of the *PcP* arrival (Figure 13b) which fixes the velocity of the ULVZ layer between 13.6 km s^{-1} (lower mantle) and 8.0 km s^{-1} (core) and provides a thickness range for the ULVZ of between 4.8 and 8.2 km. The amplitudes of the *PdP* and *PcP* phases are comparable at high frequency which further constrains the possible velocities of the two layers. As a consequence of the tuning effect in the upper, thin layer, the velocity contrast may differ by up to a factor of 2. Hence the preferred model is relatively well determined. The thickness of the ULVZ is close to the lower thickness bound reported in other areas [*Garnero et al.*, 1998]. Our preferred model consists of a 1.2 km (upper) and a 6 km (lower) layer (Figure 14). The thickness uncertainties are ±0.3 km, and the relative velocity uncertainties are ±2% or 0.2 km s^{-1} (Figures 14b and 14c). The exact parameters used are listed in Table 1. This model is an end-member model, ignoring attenuation within the low-velocity layers. If, as suggested by other studies, the ULVZ is partially molten, it should have a significantly stronger attenuation and hence lower quality factor Q than the lower mantle. Including attenuation within the ULVZ has little effect on the waveform for $Q > 150$ because of the limited thickness of the layers. At $Q < 30$, no reasonable velocities can produce an acceptable fit to the data, fixing the minimum value of Q to 30 and the minimum thickness of the ULVZ to 5.7 km (Figure 15 and Table 1). The shape of the waveform

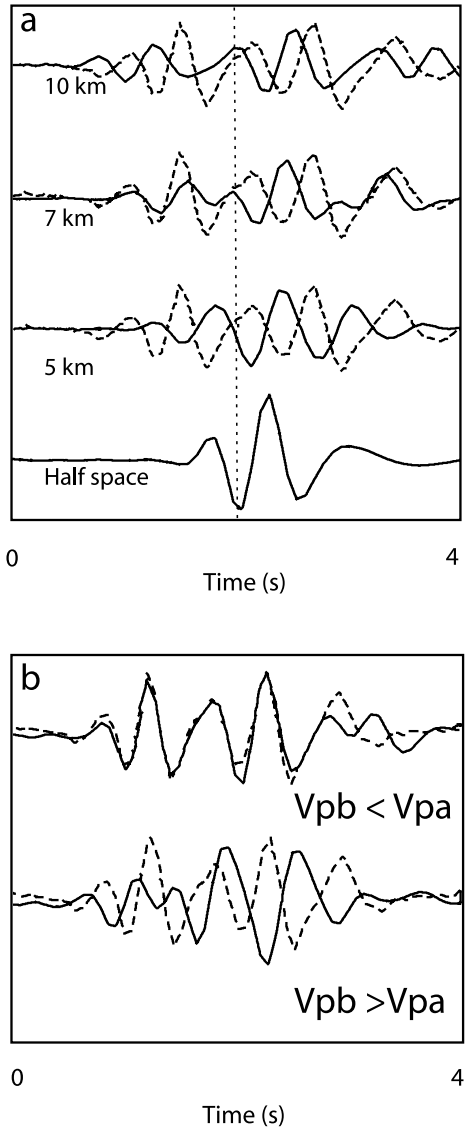

Figure 13. Results of reflectivity modeling of the stack from KRATON-1, illustrating the effect of thickness and velocity of a single layer CMB on the calculated waveform. The source waveform was extracted from the first arrivals near the source. (a) The effect of layer thicknesses between 5 and 10 km. A thickness of 7 km provides the correct duration of the waveform although not a good fit to the waveform. (b) A sequence of low-velocity decreases in the ULVZ for a double-layered CMB. This can explain the data, whereas a high-velocity layer cannot provide a fit. The observed data (dashed lines) and calculated waveforms (solid lines) are shown.

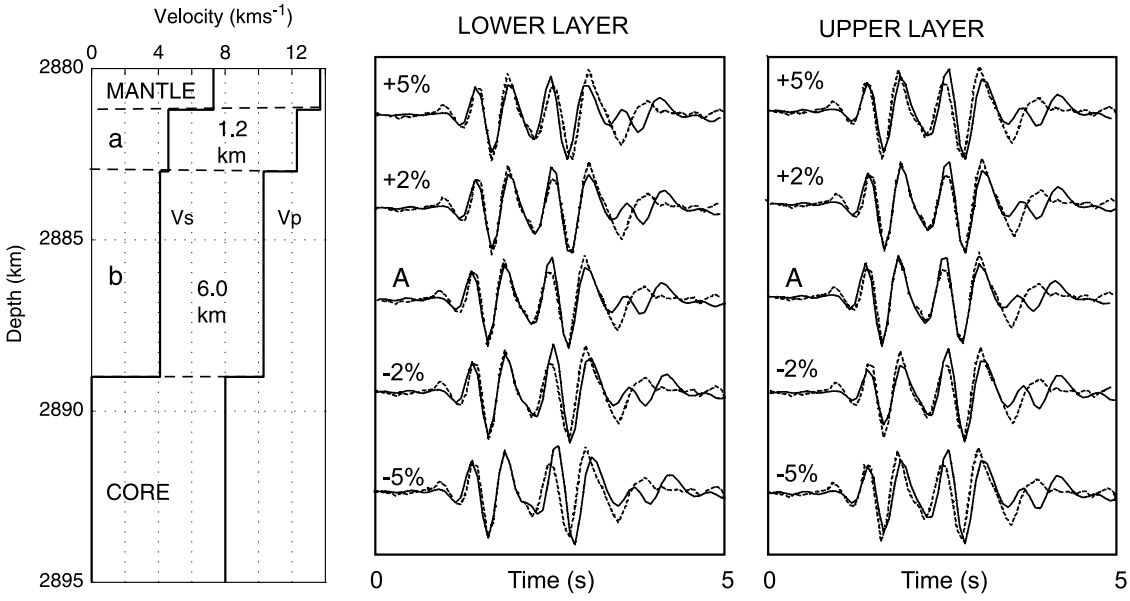

Figure 14. Results of reflectivity modeling of the stack from KRATON-1. The source waveform used for modeling was extracted from the first arrivals near the source. The length of the wave train constrains the overall thickness of the zone to around 7 km with thickness uncertainties of ±0.3 km. The stack (dashed line) and the calculated synthetics (solid line) are shown. (a) Preferred model of the CMB based on modeling of the stack from the KRATON-1 section. Velocity changes (both *P* and *S* waves) of <2% (~0.2 km s^{-1}) in the (b) lower and (c) upper layers, which do not affect the waveform significantly. However, larger velocity changes reduce the fit to the data to below acceptable levels. Abbreviation v_p is compressional velocity versus shear velocity. The parameters for model A are listed in Table 1. Abbreviations are as follows: v_p is compressional velocity, v_s is shear velocity, *a* is the upper layer within ULVZ, and *b* is the lower layer within ULVZ.

is relatively insensitive to the density within the ULVZ. We have considered models with higher densities than in the overlying lower mantle, but such models cannot explain the observations [*Thybo et al.*, 2003b]. Introducing more than two layers into the model is not supported by the available data and tends to produce internal multiples, which lengthen the wave train beyond that observed.

[36] The frequency content of the source is very important (Figure 16). The modeled 7 km thick layer becomes virtually indistinguishable from a single interface at the CMB for waveforms with a maximum frequency content of around 1.5 Hz. A higher frequency content is required in the data for such a thin layer to be observable with the velocity range at the CMB. This suggests the possible existence of a thin ULVZ layer in other regions where no precursor has been observed because the frequency content of most earthquake source signatures is relatively low. A very thin layer (0.12–0.18 km) of nonzero *S* wave velocity from a core-rigidity zone has been reported in the Tonga-Fiji region from analysis of *ScP* data [*Rost and Revenaugh*, 2001]. This layer is visible because of the extremely low *S* wave velocities in the layer.

9. Discussion

[37] Our data indicate fine structure in an extremely thin ULVZ at one location in Siberia (from profile KRATON) and lateral variability in the CMB region at another location under Siberia (from profile BATHOLITH). The character of the CMB arrival of the KRATON and the BATHOLITH profiles is different. The CMB arrival for BATHOLITH-2 is much clearer and more consistent with offset than for

Table 1. Parameters for the Models Shown in Figures 14 and 15[a]

Model	z_a, km	v_{pa}, km s^{-1}	v_{sa}, km s^{-1}	Q_{pa}	Q_{sa}	ρ_a, kg m^{-3}	z_b, km	v_{pb}, km s^{-1}	v_{sb}, km s^{-1}	Q_{pb}	Q_{sb}	ρ_b, kg m^{-3}	z_{total}, km
A	1.2	12.3	4.6	∞	∞	6.06	6.0	10.3	4.1	∞	∞	6.06	7.2
B	1.2	12.3	4.6	150	150	6.06	5.0	9.1	3.1	50	50	6.16	6.2
C	1.2	12.3	4.6	150	150	6.06	4.5	8.8	2.9	30	30	6.16	5.7
D	1.2	12.3	4.6	150	150	6.06	4.5	8.5	2.9	20	20	6.16	5.7
Mantle above the ULVZ		13.69	7.3			5.56							
Core		8.01	0.0			9.9							

[a]Letters A–D refer to examples shown in Figure 15. Model A is our preferred model shown in Figure 14. Abbreviations are as follows: *z* is thickness, v_p is compressional velocity versus shear velocity, Q_p and Q_s are quality factor, ρ is density, and v_s is shear velocity (*a* is the upper layer within ULVZ, and *b* is the lower layer within ULVZ). Subscript letters refer to upper (section a in Figure 14a) and lower (section b in Figure 14a) layers of the ULVZ. The total thickness of the ULVZ is given by z_{total}.

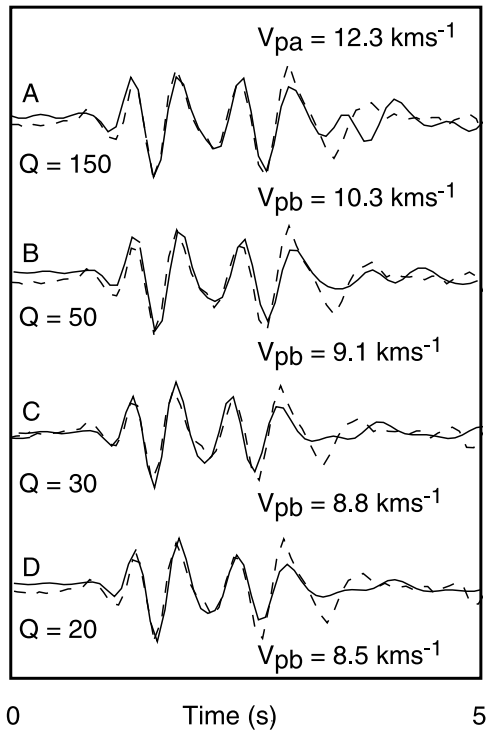

Figure 15. Modeling result of the effect of quality factor ***Q***. A unique solution does not exist because of a trade-off between Q, velocity, and the thickness of the lower layer. Model A is the best fit model shown in Figure 14. Lowering Q requires lower P and S wave velocities in the lower layer and a reduced thickness. No acceptable combination of v_p and v_s could be found for $Q < 30$ in the lower layer. The variable v_{pb} is the P wave velocity of the lower ULVZ layer. The velocity of the upper layer, v_{pa}, is 12.3 km s^{-1}. Full parameters for the various models are listed in Table 1.

KRATON. This is either because of different noise levels on the two profiles or because of different CMB structure in the two data areas. A difference in the CMB between BATHOLITH and KRATON is supported by data from other sources. Global P wave tomography modeling [*van der Voo et al.*, 1999] shows a change in the lower mantle seismic velocity at the CMB in the region of the BATHOLITH-2 profile. There is a shift from a positive velocity anomaly at the CMB beneath KRATON to a negative velocity anomaly underneath BATHOLITH. It has been suggested that this difference indicates the presence of a subducted slab from the Pacific rim subduction zones in this region. This cold slab may be cooling the lower mantle leading to an extremely thin ULVZ (or no ULVZ) underneath part of profile KRATON. Here we present evidence for the presence of a very thin ULVZ in the center part of the profile which adds constraints to the possible expected extent of the proposed slab. The lower velocities at the CMB beneath BATHOLITH suggest higher temperature than under KRATON which may allow the presence of a thick ULVZ. This is reflected in the long-duration arrivals from the CMB for this profile. We observe variations in duration of the arrivals and hence the thickness and/or physical properties of the ULVZ over distances of around 150–200 km consistent with observations from the CMB beneath the Pacific Ocean [*Williams and Garnero*, 1996; *Wysession et al.*, 1999]. These variations are possibly sharp enough to generate diffractions at the edges of the separate regions. However, several different mechanisms could be responsible for some of our observations, although a variable, multilayered ULVZ provides the best explanation of our observations.

[38] Though nonunique, our waveform modeling suggests that velocities in the ULVZ are very low with velocity reductions of −10% for P waves and −37% for S waves in the upper layer and 25% for P waves and −45% for S waves in the lower layer of the ULVZ at the CMB below KRATON-1. The values for the upper layer are consistent with previous estimates for ULVZ velocity reductions of −10% for P waves and −30% for S waves [*Garnero et al.*, 1998]. Taking the uncertainties in the fit for the best model into account, the velocity reduction in the lower layer could be as little as 23% and 43% for P and S waves, respectively. These velocity reductions are larger than most previous studies. However, analysis of *SPdKS* beneath the Pacific ocean and recorded in North America shows P wave velocity reductions of 18% for P waves and 50% for S waves [*Rondenay and Fischer*, 2002, 2003], which are very close to our values. This study also suggests the existence of a two-layer ULVZ. These low velocities are within acceptable possible velocities for reasonable amounts of partial melt for S waves (Figure 17) with the exact amount of partial melt being dependent on the exact melt geometry [*Mavko*, 1980]. However, the P wave velocity in the lower layer is outside the predicted range of velocities for the

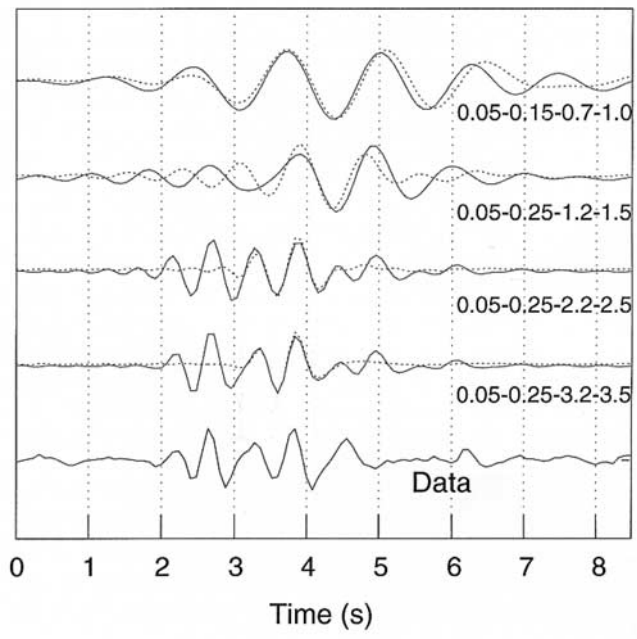

Figure 16. Illustration of the importance of the frequency content of the source waveform for identification of a thin ULVZ. The result of reflectivity calculations for a single interface (dashed line) and the data after bandpass filtering (solid line) are shown, with the frequency characteristics listed to the right of the figure. For frequencies <1 Hz the thin ULVZ becomes indistinguishable from a CMB with no ULVZ present.

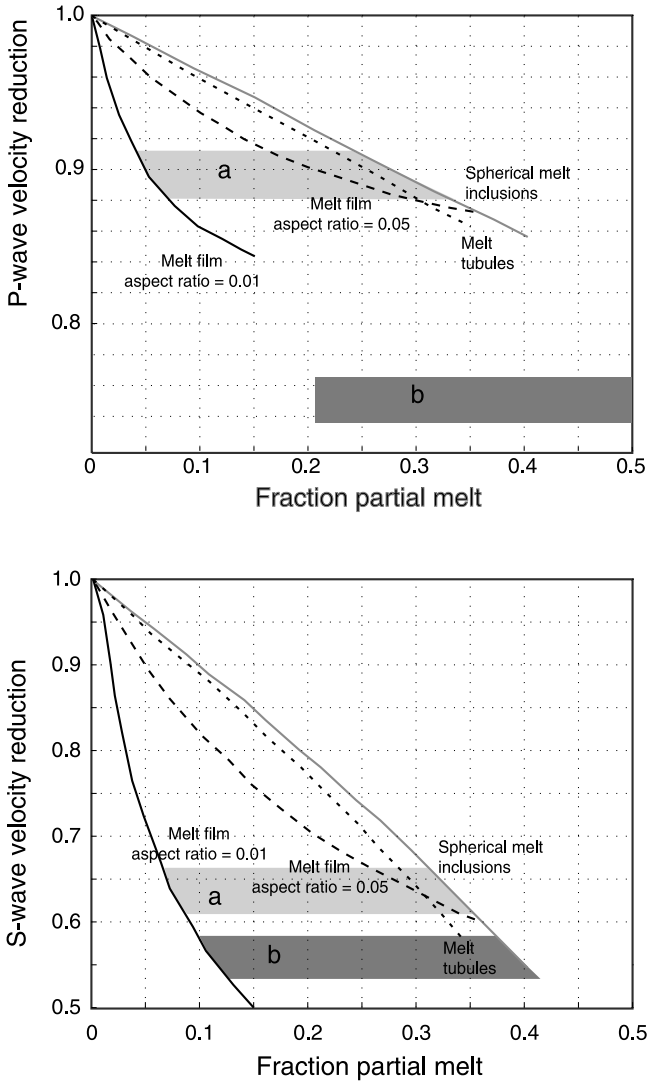

Figure 17. Estimates of the amount of partial melt in the ULVZ and a comparison of results of this analysis with those of *Williams and Garnero* [1996] for varying melt geometries. Our results for *P* waves (error bounds indicated by the shaded boxes) lie within the possible values for various types of melt geometries in our uppermost layer (shaded region a) but are much lower than they allow for the lowermost layer (shaded region b). Both *S* wave estimates fit within the data bounds and suggest possible melt fractions of over 30% and up to 50% depending on the exact melt geometry in the layer.

modeling by *Williams and Garnero* [1996]. Although not consistent with the partial melt modeling, these values are not outside the range of previously modeled ULVZ parameters, especially for thin ULVZs where a trade-off between *P* wave velocity and thickness exists [*Revenaugh and Meyer*, 1997; *Garnero and Helmberger*, 1998]. One possible explanation for the very low velocities is sedimentation of light silicic material at the CMB which would produce a very low velocity layer with velocity reductions of 25% for *P* waves and 50% for *S* waves [*Buffett et al.*, 2000].

[39] The difference between the two layers could therefore represent either a change in the percentage of partial melt or, possibly, of the melt geometry (a cumulate layer at the top of a high-percentage melt layer may be a possibility). The two layers could also be a combination of partial melt and other low-velocity material such as silicic sediments. In our upper layer, partial melt percentages could be between 5% and 30%. The extremely low velocities in the lower layer are consistent with percentages of melt from 15% to 40% [*Williams and Garnero*, 1996]. The density of mantle melts at very high temperature and pressure is higher than the surrounding matrix [*Rigden et al.*, 1984, 1989] such that any melt would sink to the bottom of the melt layer. This would be consistent with a two-layer model with a higher percentage of melt in the lower layer of the ULVZ than at the top of the ULVZ.

10. Conclusions

[40] We observe clear seismic phases from the core-mantle boundary on high-density record sections from three nuclear explosions in Siberia. The arrival times and move-out velocities of these phases are consistent with the expected reflection times from the CMB of the *PcP* phase. On one profile the observation is made on reversed record sections. Hence we are confident that the seismic phases originate from the CMB.

[41] The long waveform and a complex precursor (*PdP*) to the *PcP* reflection from the CMB demonstrate the presence of an ULVZ under Siberia, where previous interpretations indicate that such a zone is absent. The complexity of the phases indicate additional structure within the ULVZ at one location. It has been suggested that the complexity is caused by effects of the seismic source, such as ghosts or collapse and spalling of the cavity produced by the powerful explosions. However, our observations show that such causes can be ruled out, and the observation requires the presence of an ULVZ. Observations on the global seismograph network of signals from several nuclear explosions confirm a strong lateral variability in the CMB phases.

[42] The modeled velocities in the CMB under Siberia are consistent with the presence of high percentages (10–40%) of partial melt in the ULVZ and decreasing melt percentage with distance from the CMB. Our discovery of a complex ULVZ under Siberia suggests that the CMB may generally be complex and that it may exist in a larger part of the Earth than hitherto suggested (12%). Our observations demonstrate high lateral variability of the properties of the ULVZ.

[43] **Acknowledgments.** This work was supported by funds from the Carlsberg Fund, Copenhagen, Denmark, and the Danish National Research Council. We would also like to thank GEON Center in Moscow for providing the data. We thank Jan Fyen for providing the data from NORSAR. Data from the Gräfenberg array were provided by the Seismological Central Observatory (SZGRF). Data for other seismic stations were acquired from the IRIS DMC. Reviews from Ed Garnero and an anonymous reviewer greatly improved our manuscript.

References

Ake, J. P., and A. R. Sanford (1988), New evidence for the existence and internal structure of a thin layer of magma at mid-crustal depths near Socorro, New Mexico, *Bull. Seismol. Soc. Am.*, *78*(3), 1335–1359.

Astiz, L., P. Earle, and P. Shearer (1996), Global stacking of broadband seismograms, *Seismol. Res. Lett.*, *67*(4), 8–18.

Buffett, B. A., E. J. Garnero, and R. Jeanloz (2000), Sediments at the top of Earth's core, *Science*, *290*(5495), 1338–1342.

Castle, J. C., and R. D. van der Hilst (2000), The core-mantle boundary under the Gulf of Alaska; No ULVZ for shear waves, *Earth Planet. Sci. Lett.*, *176*(3–4), 311–321.

Crotwell, H. P., T. J. Owens, and J. Ritsema (1999), The TauP toolkit; Flexible seismic travel-time and ray-path utilities, *Seismol. Res. Lett.*, *70*(2), 154–160.

Egorkin, A. V. (1999), Study of the mantle on super long-range geotraverses, *Izv. Russ, Acad. Sci. Phys. Solid Earth, Eng. Transl.*, *35*(7–8), 630–645.

Freybourger, M., F. Krueger, and U. Achauer (1999), A 22 degrees long seismic profile for the study of the top of *D″*, *Geophys. Res. Lett.*, *26*(22), 3409–3412.

Freybourger, M., S. Chevrot, F. Kruger, and U. Achauer (2001), A waveform migration for the investigation of *P* wave structure at the top of *D″* beneath northern Siberia, *J. Geophys. Res.*, *106*(3), 4129–4140.

Fuchs, K. (1997), *Upper Mantle Heterogeneities From Active and Passive Seismology*, 366 pp., Kluwer Acad., Norwell, Mass.

Fuchs, K., and G. Mueller (1971), Computation of synthetic seismograms with the reflectivity method and comparison with observations, *Geophys. J. R. Astron. Soc.*, *23*(4), 417–433.

Gaherty, J. B., and T. Lay (1992), Investigation of laterally heterogeneous shear velocity structure in *D′* beneath Eurasia, *J. Geophys. Res.*, *97*(1), 417–435.

Garnero, E. J., and D. V. Helmberger (1995), A very slow basal layer underlying large-scale low-velocity anomalies in the lower mantle beneath the Pacific; Evidence from core phases, *Phys. Earth Planet. Inter.*, *91*(1–3), 161–176.

Garnero, E. J., and D. V. Helmberger (1996), Seismic detection of a thin laterally varying boundary layer at the base of the mantle beneath the central Pacific, *Geophys. Res. Lett.*, *23*(9), 977–980.

Garnero, E. J., and D. V. Helmberger (1998), Further structural constraints and uncertainties of a thin laterally varying ultralow-velocity layer at the base of the mantle, *J. Geophys. Res.*, *103*(6), 12,495–12,509.

Garnero, E. J., and R. Jeanloz (2000), Fuzzy patches on the Earth's core-mantle boundary?, *Geophys. Res. Lett.*, *27*(17), 2777–2780.

Garnero, E. J., and J. E. Vidale (1999), *ScP*; A probe of ultralow velocity zones at the base of the mantle, *Geophys. Res. Lett.*, *26*(3), 377–380.

Garnero, E. J., S. P. Grand, and D. V. Helmberger (1993), Low *P* wave velocity at the base of the mantle, *Geophys. Res. Lett.*, *20*(17), 1843–1846.

Garnero, E. J., J. Revenaugh, Q. Williams, T. Lay, and L. H. Kellogg (1998), Ultralow velocity zone at the core-mantle boundary, in *The Core-Mantle Boundary Region*, edited by M. Gurnis et al., pp. 319–334, AGU, Washington, D. C.

Grand, S. P., R. D. van der Hilst, and S. Widiyantoro (1997), Global seismic tomography; A snapshot of convection in the Earth, *GSA Today*, *7*(4), 1–7.

Helmberger, D. V., L. Wen, and X. Ding (1998), Seismic evidence that the source of the Iceland hotspot lies at the core-mantle boundary, *Nature*, *396*(6708), 251–255.

Helmberger, D., S. Ni, L. Wen, and J. Ritsema (2000), Seismic evidence for ultralow-velocity zones beneath Africa and eastern Atlantic, *J. Geophys. Res.*, *105*(10), 23,865–23,878.

Kampfmann, W., and G. Mueller (1989), *PcP* amplitude calculations for a core-mantle boundary with topography, *Geophys. Res. Lett.*, *16*(7), 653–656.

Kennett, B. L. N., and E. R. Engdahl (1991), Travel times for global earthquake location and phase identification, *Geophys. J. Int.*, *105*(2), 429–465.

Knittle, E. (1998), The solid/liquid partitioning of major and radiogenic elements at lower mantle pressures; Implications for the core-mantle boundary region, in *The Core-Mantle Boundary Region*, edited by M. Gurnis et al., pp. 119–130, AGU, Washington, D. C.

Mavko, G. M. (1980), Velocity and attenuation in partially molten rocks, *J. Geophys. Res.*, *85*(B10), 5173–5189.

Mori, J., and D. V. Helmberger (1995), Localized boundary layer below the mid-Pacific velocity anomaly identified from a *PcP* precursor, *J. Geophys. Res.*, *100*(10), 20,359–20,365.

Morozova, E. A., I. B. Morozov, S. B. Smithson, and L. Solidilov (2000), Lithospheric boundaries and upper mantle heterogeneity beneath Russian Eurasia; Evidence from the DSS profile QUARTZ, *Tectonophysics*, *329*(1–4), 333–344.

Murphy, J. R., I. O. Kitov, B. W. Barker, and D. D. Sultanov (2001), Seismic source characteristics of Soviet peaceful nuclear explosions, *Pure Appl. Geophys.*, *158*(11), 2077–2101.

Nielsen, L., H. Thybo, and L. Solidilov (1999), Seismic tomographic inversion of Russian PNE data along profile Kraton, *Geophys. Res. Lett.*, *26*(22), 3413–3416.

Nielsen, L., H. Thybo, and A. V. Egorkin (2002), Implications of seismic scattering below the 8 degrees discontinuity along PNE profile Kraton, *Tectonophysics*, *358*(1–4), 135–150.

Reasoner, C., and J. Revenaugh (2000), *ScP* constraints on the ultralow-velocity zone density and gradient thickness beneath the Pacific, *J. Geophys. Res.*, *105*(12), 28,173–28,182.

Revenaugh, J., and R. Meyer (1997), Seismic evidence partial melt within a possibly ubiquitous low-velocity layer at the base of the mantle, *Science*, *277*(5326), 670–673.

Rigden, S. M., T. J. Ahrens, and E. M. Stolper (1984), Densities of liquid silicates at high pressures, *Science*, *226*(4678), 1071–1074.

Rigden, S. M., T. Ahrens, and E. M. Stolper (1989), High-pressure equation of state of molten anorthite and diopside, *J. Geophys. Res.*, *94*(7), 9508–9522.

Rondenay, S., and K. M. Fischer (2002), Local constraints on CMB structure from multichannel, broadband SKS-coda analysis, *Eos Trans. American Geophysical Union*, *83*(47), *Fall Meet Suppl.*, Abstract S22A-1004.

Rondenay, S., and K. M. Fischer (2003), Constraints on localized core-mantle boundary structure from multichannel, broadband *SKS* coda analysis, *J. Geophys. Res.*, *108*(B11),2537, doi:10.1029/2003JB002518.

Rost, S., and J. Revenaugh (2001), Seismic detection of rigid zones at the top of the core, *Science*, *294*(5548), 1911–1914.

Ryberg, T., and F. Wenzel (1999), High-frequency wave propagation in the uppermost mantle, *J. Geophys. Res.*, *104*(5), 10,655–10,666.

Stutzmann, E., L. Vinnik, A. Ferreira, and S. Singh (2000), Constraint on the *S* wave velocity at the base of the mantle, *Geophys. Res. Lett.*, *27*(11), 1571–1574.

Sultanov, D. D., J. R. Murphy, and K. D. Rubinstein (1999), A seismic source summary for Soviet peaceful nuclear explosions, *Bull. Seismol. Soc. Am.*, *89*(3), 640–647.

Sylvander, M., and A. Souriau (1996), *P*-velocity structure of the core-mantle boundary region inferred from PKP (AB)-PKP (BC) differential travel times, *Geophys. Res. Lett.*, *23*(8), 853–856.

Sylvander, M., B. Ponce, and A. Souriau (1997), Seismic velocities at the core-mantle boundary inferred from *P* waves diffracted around the core, *Phys. Earth Planet. Inter.*, *101*(3–4), 189–202.

Thomas, C., and M. Weber (1997), *P* velocity heterogeneities in the lower mantle determined with the German Regional Seismic Network; Improvement of previous models and results of 2D modelling, *Phys. Earth Planet. Inter.*, *101*(1–2), 105–117.

Thomas, C., M. Weber, A. Agnon, and A. Hofstetter (1998), A low-velocity lamella in *D″*, *Geophys. Res. Lett.*, *25*(15), 2885–2888.

Thomas, C., J. M. Kendall, and M. Weber (2002), The lowermost mantle beneath northern Asia; I, Multi-azimuth studies of a *D″* heterogeneity, *Geophys. J. Int.*, *151*(1), 279–295.

Thybo, H., and E. Perchuc (1997), The seismic 8 degrees discontinuity and partial melting in continental mantle, *Science*, *275*(5306), 1626–1629.

Thybo, H., E. Perchuc, and L. Nielsen (2003a), Heterogeneity at the top of the Earth's transition zone from lower upper mantle reflectivity, *Earth Planet. Sci. Lett.*, *16*(3), 259–269.

Thybo, H., A. R. Ross, and A. V. Egorkin (2003b), Explosion seismic reflections from the Earth's core, *Earth Planet. Sci. Lett.*, *216*(4), 693–702.

van der Hilst, R. D., S. Widiyantoro, and E. R. Engdahl (1997), Evidence for deep mantle circulation from global tomography, *Nature*, *386*(6625), 578–584.

van der Voo, R., W. Spakman, and H. Bijwaard (1999), Mesozoic subducted slabs under Siberia, *Nature*, *397*(6716), 246–249.

Vidale, J. E., and M. A. H. Hedlin (1998), Evidence for partial melt at the core-mantle boundary north of Tonga from the strong scattering of seismic waves, *Nature*, *391*(6668), 682–685.

Weber, M. (1993), *P*- and *S*-wave reflections from anomalies in the lowermost mantle, *Geophys. J. Int.*, *115*(1), 183–210.

Weber, M., and J. P. Davis (1990), Evidence of a laterally variable lower mantle structure from *P*- and *S*-waves, *Geophys. J. Int.*, *102*(1), 231–255.

Wen, L., and D. V. Helmberger (1998), Ultra-low velocity zones near the core-mantle boundary from broadband PKP precursors, *Science*, *279*(5357), 1701–1703.

Williams, Q., and E. J. Garnero (1996), Seismic evidence for partial melt at the base of Earth's mantle, *Science*, *273*(5281), 1528–1530.

Williams, Q., J. Revenaugh, and E. Garnero (1998), A correlation between ultra-low basal velocities in the mantle and hot spots, *Science*, *281*(5376), 546–549.

Wysession, M. E., A. Langenhorst, M. J. Fouch, E. G. I. Al, P. J. Shore, and T. J. Clarke (1999), Lateral variations in compressional/shear velocities at the base of the mantle, *Science*, *284*(5411), 120–125.

A. R. Ross and H. Thybo, Geological Institute, University of Copenhagen, Øster Voldgade 10, Copenhagen, DK-1350, Denmark. (ross@seis.geol.ku.dk; thybo@geol.ku.dk)

L. N. Solidilov, Center for Regional Geophysical and Geoecological Studies (GEON), Chistyi per. 4, Moscow, 119034 Russia. (moscow@geon.msk.su)